Journal of Climate

# The partitioning of meridional heat transport from the Last Glacial Maximum to CO2 quadrupling in coupled climate models

--Manuscript Draft--

| | |
|---|---|
| **Manuscript Number:** | JCLI-D-19-0797 |
| **Full Title:** | The partitioning of meridional heat transport from the Last Glacial Maximum to CO2 quadrupling in coupled climate models |
| **Article Type:** | Article |
| **Corresponding Author:** | Aaron Donohoe, Ph.D.<br>University of Washington<br>Seattle, WA UNITED STATES |
| **Corresponding Author's Institution:** | University of Washington |
| **First Author:** | Aaron Donohoe, Ph.D. |
| **Order of Authors:** | Aaron Donohoe, Ph.D. |
| | Kyle C Armour |
| | Gerard H Roe |
| | David S. Battisti |
| | Lily C Hahn |
| **Abstract:** | Meridional heat transport (MHT) is analyzed in ensembles of coupled climate models simulating climate states ranging from the Last Glacial Maximum (LGM) to quadrupled CO 2 . MHT is partitioned here into atmospheric (AHT) and implied oceanic (OHT) heat transports. In turn, AHT is partitioned into dry and moist energy transport by the meridional overturning circulation (MOC), transient eddy energy transport (TE) and stationary eddy energy transport (SE) using only monthly averaged model output that is typically archived. In all climate models examined, the maximum total MHT (AHT+OHT) is nearly climate-state invariant, except for a modest (4%, 0.3PW) enhancement of MHT in the Northern Hemisphere (NH) during the LGM. However, the partitioning of MHT depends markedly on the climate state and the changes in partitioning differs considerably among different climate models. In response to CO 2 quadrupling, poleward implied OHT decreases while AHT increases by a nearly compensating amount. The increase in annual-mean AHT is a smooth function of latitude but is due to a spatially inhomogeneous blend of changes in SE and TE which vary by season. During the LGM, the increase in wintertime SE transport in the NH mid-latitudes exceeds the decrease in TE resulting in enhanced total AHT. Total AHT changes in the SH are not significant. These results suggest that the net top of atmosphere radiative constraints on total MHT are relatively invariant to climate forcing due to nearly compensating changes in absorbed solar radiation and outgoing longwave radiation. However, the partitioning of MHT depends on detailed regional and seasonal factors. |

We thank all three Reviewer's and the Editor for their thorough and thoughtful critiques. We list the reviewer's/editor's comments in red and our responses in black.

EDITOR COMMENTS:

While two of the three reviewers recommend major revision, few if any of their comments require major changes to the computations, so i have settled on minor revision instead. An exception might be the concern that one of the reviewers has regarding models that do not conserve energy adequately, but I feel that some additional text addressing this concern would be sufficient, with more emphasis on what additional considerations are required if there is inadequate conservation in the underlying model.

Please see our response to Reviewer 1 major point 2 for an extensive discussion. In short, we apply adjustments to account for lack of energy and mass conservation in climate models. This technique appears to be working in the model used to validate our technique (NCAR CESM) which does not conserve mass and energy on the output grid that we use to validate our technique.

Perhaps most importantly, all three reviewers, from different perspectives, feel that the references to the literature are not fully adequate and make suggested additions that you should consider carefully.

We thank all three Reviewers for pointing us toward pertinent literature that we neglected to cite in the original manuscript. We have added citations to the theoretical work on Bjerknes compensation (as requested by Reviewer 1), model simulations that have addressed mechanisms of MHT invariance (as requested by Reviewer 2) and the studies that diagnose transient eddy heat transport as a residual (as requested by Reviewer 3).

I also sympathize with the comments of the reviewer who has focused on the technical aspects of the flux decomposition and does not understand exactly what is distinctive about the methodology here in the context of the existing literature.

Please see response to Reviewer 3 major point 1. In short, we agree that similar residual methods have been used to diagnose transient eddy energy and moisture transports in single model studies (we now cite these studies). Our work applies these techniques across a large model ensemble and employs a different technique to adjust for conservation of mass and energy.

Following one of the reviewers, I also think you want to avoid raising Stone's prescription as a straw man which you then show is inadequate in some cases. Few readers, i suspect, will come to this paper with a preconception that Stone's argument is

fundamental rather than an approximation in a limited parameter range. I guess the goal should be to help delineate the parameter regime in which it is useful.

Thank you for this suggestion. We have backed off using Stone's argument as a straw man. Please see our extensive response to Reviewer 2's criticism and the revised discussion section.

I am also sympathetic to the concerns that the density of acronyms in some paragraphs make the discussion difficult to follow,

We have added written out key acronyms in selected paragraphs throughout the manuscript to remind the reader of the acronym's meaning. We hope this improves the manuscript's readability.

and that the captions should have clear warnings when subpanels in the same figures have different ranges in their vertical axes.

We have revised the axes on all 10 main manuscript figures to achieve more consistency between figures and subpanels. In the revised figure captions, we also warn of differences in axis.

Concerning the length of the paper, I won't enforce J.Climate's length limit, but I think most readers would prefer a more succinct summary and conclusions section, performing some triage to emphasize the major messages.

We have reduced the repetitive discussions. We appreciate the Editor's leniency on the length limit and hope that the reader will benefit from having the partitioning technique, observational comparison, model results and discussion of mechanisms in a single manuscript.

Reviewer 1 -- Major comments:

1. Long sentences: it seems that the authors like to use long sentences in this work, which seriously reduce the readability of this manuscript. For example,

Abstract: statement in line 18-21, 35 words; line 21-25, 44 words.

This sentence has been split into two sentences in the revised manuscript.

Introduction: line 42-45;

While this sentence is long, we feel it appropriately introduces the concept and the numerous modifiers are necessary for scientific accuracy.

line 49-53;

This sentence has been split into two sentences in the revised manuscript.

line 54-59;

This sentence uses a colon to introduce series of items and is grammatically correct.

line 60-62;

This sentence is not very long.

line 121-124.

This sentence has been split into two sentences in the revised manuscript.

Data and methods: line 298-290;

This sentence (lines 284-290) has been split into two sentences in the revised manuscript.

line 305-308;

This sentence has been rewritten in the revised manuscript.

line 309-312.

This sentence has been rewritten in the revised manuscript.

Section 3: line 327-330;

This sentence has been rewritten in the revised manuscript.

line 333-336;

This sentence uses a colon to separate two independent clauses and is grammatically correct.

line 390-393.

This sentence has been split into three sentences in the revised manuscript.

Section 6: line 522-525;

Although this sentence is long, we believe all the modifiers are necessary to point the reader to the scientific result we are highlighting.

Section 7: line 568-571;

This sentence has been split into two sentences in the revised manuscript.

2. Section 2c: Conservation of energy is critical to the validation of the technique used in this work. CESM coupled model is doing very well in both the energy conservation and mass conservation. We knew it, since we also have check the conservation problem carefully in our previous studies. However, many coupled models used in CMIP5, as far as I know, are not doing well in the conservations of energy and mass. The portioning technique itself used in this work has no problem, but it is not suitable to the models that mass and energy are not conserved. Therefore, I strongly suggest that only the models with good conservation can be used in this study, and other models without conservation should be excluded! I think this should a fundamental rule. Since the MHT (AHT and OHT) is an integrated quantity, conservations of energy and mass are particularly important to them. I cannot believe the mixture of "right" and "wrong" results.

We agree that conservation of mass and energy pose potential problems for the calculation of and partitioning of MHT in both climate models and observations. Our MHT and AHT partitioning technique makes two adjustments to account for the lack of energy and mass conservation in both models and observations (as described in the data and methods section of the manuscript):

**Energy conservation:** The global mean TOA radiative imbalance is removed by making a spatially invariant adjustment to the net radiation at all locations prior to calculating MHT via Eq. 2. Similarly, the global mean net surface energy flux is removed by making a spatially invariant adjustment to the net surface energy flux at all locations prior to calculating the (implied) OHT. This procedure produces AHT and OHT curves that are equal to zero and both poles independent of whether the integral in Eq. 2 is performed starting at the North Pole or the South Pole. This approach inherently assumes that the lack of energy conservation in climate models and observational data sets is spatially homogeneous. While there is no formal justification for this assumption, we know of no work that has analyzed the spatial structure of energy losses in climate models or the spatial decorrelation length scale of uncertainty in observational radiation data. The spatial structure of non-energy conserving processes is vital to understanding their impact on the calculation of MHT and AHT: processes that are globally homogenous (such as absolute calibration of satellite measurements) have no impact on MHT, while processes that vary at the gridpoint scale make a modest contribution to AHT error. Processes that violate energy conservation that project on a regional scale (i.e. that project onto the equator-to-pole scale) make the largest contribution to AHT error (see Wunsch (2005) for a thorough discussion).

As noted by the Reviewer and expanded on by Lucarini and Ragone (2011), pre-industrial control simulations in coupled climate models have unrealistically large energy imbalances of order 1 W $m^{-2}$. In the 10 year long CESM pre-industrial simulation that was used to validate our partitioning technique (Section 2C of the manuscript), the global mean TOA radiative imbalance is 1.2 W $m^{-2}$ with a 0.5 W $m^{-2}$ imbalance in the atmosphere and 0.7 W $m^{-2}$ in the ocean (diagnosed from the net energy flux at the surface). We note that this global mean imbalance seems to differ from that reported by Forster et al. (2013) for CESM1 and it is unclear if the difference is due to the relatively short duration of the run we analyzed or differences in the exact model parameters used. The energy imbalance in the CESM control run that we analyzed is typical for the CMIP5 pre-industrial simulations analyzed in this study which, on average, have an absolute global TOA imbalance of 0.8 W $m^{-2}$ and an atmospheric imbalance of 1.0 W $m^{-2}$. It is reassuring, then, that the AHT in CESM calculated using a spatially invariant adjustment is virtually identical to that calculated explicitly from the model output. This agreement suggests that the lack of energy conservation in the CESM is not due to errors that occur on the equator-to-pole scale, and we see no reason why this should not be the case for other CMIP5 models.

Additionally, Hobbs et al. (2016) found that the lack of energy conservation is nearly time and climate state invariant in each GCM especially in the atmosphere. Below, we compare the global mean atmospheric energy in balance in the preindustrial simulation compared to that in the $4XCO_2$ and LGM simulation in the same model (Fig. R1). The clustering of all simulations near the 1:1 line suggests that the lack of energy conservation in each model is nearly unchanged across the simulations analyzed. Thus, we do not expect the lack of energy conservation to impact our calculations of the changes in AHT partitioning.

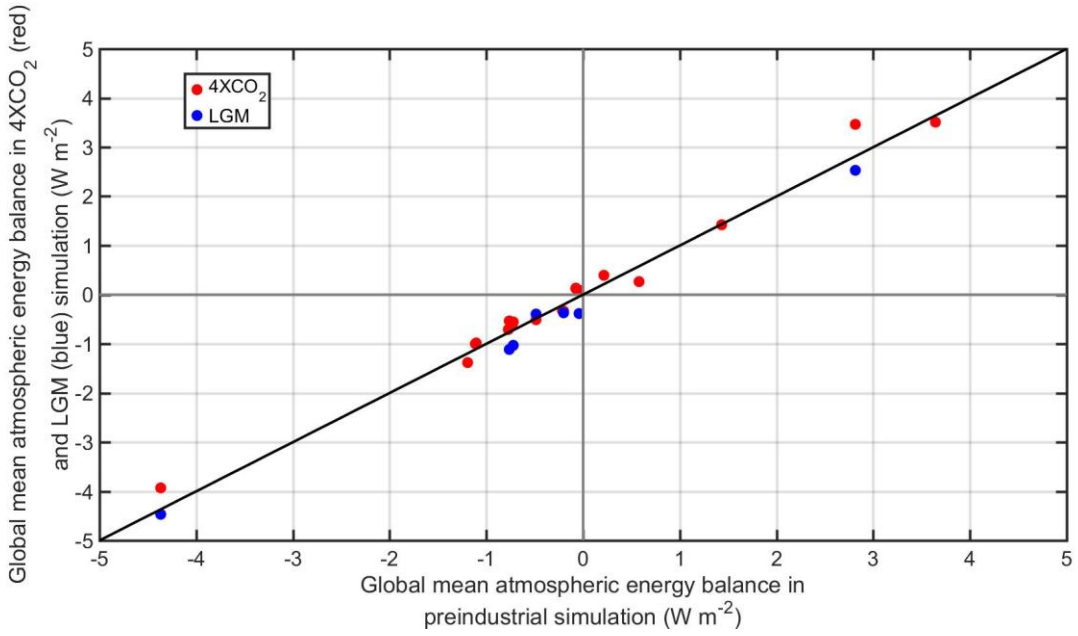

**Figure R1. The global mean energy imbalance in the atmosphere in the (abscissa) 4X$CO_2$ simulations (red) and LGM simulations (blue) compared to that in the preindustrial simulation in the same model (ordinate). The 1:1 line is shown in black.**

While we appreciate the Reviewer's concern that some climate models have very large pre-industrial global mean energy imbalances (three models have absolute values > 3 W $m^{-2}$) we are reluctant to discard these models from our MHT calculations without an additional understanding of the nature and spatial structure of the non-energy conserving processes. Specifically, it is possible that some models have a small global energy imbalance as a result of compensating non-conservative processes that are regional in nature and, thus, would have substantial impacts on the MHT calculation. Therefore, we are reluctant to use global mean energy imbalance as a litmus test for the validity of the MHT calculation.

We also note that the lack of energy conservation in climate models is small compared to the observational uncertainty on satellite measurements of global TOA energy imbalance that are used to calculate observational based MHT. The raw CERES data has a net global mean energy imbalance of order 5 W $m^{-2}$ (Loeb et al. 2009). We use the CERES EBAF data which makes reasonable adjustments to the parameters in the CERES retrieval algorithm to best match the global mean energy imbalance implied from decadal ocean heat uptake (central estimate of 0.71 W $m^{-2}$). The spatial structure of these adjustments and the associated uncertainty in calculated MHT and AHT are active areas of research and debate that are beyond the scope of the present manuscript. Because the largest source of uncertainty in the satellite observations is believed to be absolute calibration error, it is likely that the satellite-derived global mean energy imbalance is not more problematic than that in models (at least, as far as AHT calculations are concerned). We mention this here just to point out that the lack of energy conservation in climate models is not unique to models; it is a pervasive and unresolved issue in climate science. We believe we have dealt with this issue to best of our ability given our current understanding of the underlying issues.

**Mass conservation:** We adjust for lack of mass conservation in the atmosphere by removing the (mass weighted) vertical average moist static energy (separately for latent, sensible and potential energy) at each latitude. This technique was developed by Donohoe and Battisti (2012) and expanded on by Liang et al. (2018). In short, that technique calculates energy flux divergences in the atmosphere by calculating the MSE contrast between the poleward and equatorward moving air and implicitly balances the mass budget of the atmosphere. We find this technique preferable to the conventional mass adjustment by a barotropic wind correction (Trenberth and Stepanaiak, 2003) which has been demonstrated to depend on the reference state of the atmosphere and the consistency of reference state across the ocean and atmosphere (Mayer et el. 2017). The validation of this technique in CESM (Section 2c) suggests that our methodology is working extremely well for both energy and moisture transport.

3. This work is lack of some fundamental understanding of compensation physics. Previous theoretical studies have suggested that, in a world with energy and mass conservation,

the changes in AHT and OHT have to compensate with each other. The compensation rate is determined by internal parameters of the Earth system. In a world without conservations, the changes in AHT and OHT do not have to compensate with each other, and they tend to be collaborated, for example, in a world with strong global warming forced by 4xCO2. Please refer to the recent works listed below:

We apologize for failing to cite these very relevant publications and thank the Reviewer for pointing us toward this set of papers. We discuss these works in the Discussion section of the revised manuscript and where the concept of diffusion of moist static energy is used.

1) Liu, Z., C. He, and F. Lu, 2018: Local and Remote Responses of Atmospheric and Oceanic Heat Transports to Climate Forcing: Compensation versus Collaboration. J. Climate, 31, 6445-6460. doi: 10.1175/JCLI-D-17-0675.1.
Discussed and cited in reference to the compensation of AHT and OHT expected in the limit of efficient atmospheric dynamics.

2) Liu, Z., H. Yang, C. He, and Y. Zhao, 2016: A theory for Bjerknes compensation: the role of climate feedback. J. Climate, 29(1), 191-208. doi: 10.1175/JCLI-D-15-0227.1.
Cited when the concept of MSE diffusion is first introduced.

3) Yang, H., Y. Zhao, and Z. Liu, 2016: Understanding Bjerknes compensation in atmosphere and ocean heat transports using a coupled box model. J. Climate, 29(6), 2145-2160, doi: 10.1175/JCLI-D-15-0281.1.
Discussed and cited in the discussion of the relative roles of radiation and MHT in damping external forcing.

4) Yang, H., Y. Zhao, Q. Li, and Z. Liu, 2015: Heat transport in atmosphere and ocean over the past 22,000 years. Nature Scientific Reports, 5: 16661. doi: 10.1038/srep16661
Discussed and cited in the discussion of the relative roles of radiation and MHT in damping external forcing.

4. Under 4xCO2, an increase in poleward TE in the SH storm track region (30S-60S) occurs during all seasons. The reason to this change is not answered in this work. Please deliberate it.

Thank you for pointing this out. The meridional temperature gradient increases slightly in this region (during all seasons) as a result of delayed Southern Ocean warming (see Figure R2 below for annual mean plot). Because moisture is preferentially loaded in the lower latitudes, the moisture (and moist static energy) gradient is enhanced relative to the pre-industrial. We speculate that the increased poleward transient eddy (TE) moisture transport follows the enhanced moisture gradient in this region. We have added a brief discussion to the revised manuscript.

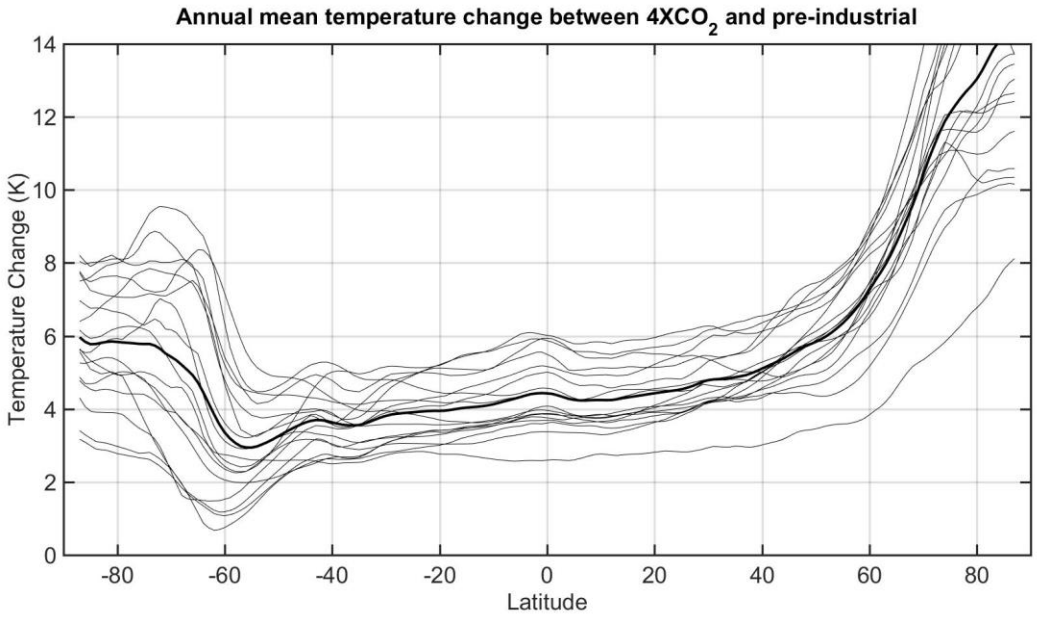


**Figure R2. The meridional structure of the surface temperature change in the $4XCO_2$ simulations. Thin lines show individual models and the thick line shows the ensemble average. Note that the equator-to-pole temperature gradient decreases throughout the Northern Hemisphere but increases in the region from 30S to 60S.**

5. The compensation changes in the component of AHT are also noticed earlier in Yang and Dai (2015) (Effect of wind forcing on the meridional heat transport in a coupled model: equilibrium response. Climate Dynamics, 45(5): 1451-1470, doi: 10.1007/s00382-014-2393-0.) For example, the good compensation changes between the mean dry static energy (DSE) and mean latent energy (LE) within the tropics (because stronger HC means the stronger equatorward convergence of the water vapour), and the perfect compensation between the mean and eddy DSE transports in the extratropics (as a result of the equatorward shift of the Ferrell Cell and enhancement of atmospheric baroclinicity in the mid-high latitudes, particularly over the North Atlantic).

Cited in the revised manuscript in discussion of the moist/dry partitioning changes in the tropical MOC.

6. By analyzing ensembles of CMIP5 models, the authors should also notice that the Earth's climate is trying to maintain the balance between two hemispheres. If the ocean in the NH is colder than that in the SH (may be due to the reduced northward heat transport cross the Equator in the Atlantic), the atmosphere would respond to the ocean with colder temperature in the SH than in the NH by transporting more heat northward cross the equator over the Pacific. It is pity that the authors did not delve into the compensation changes between two hemispheres.

We agree that the inter-hemispheric energy transport is a fascinating topic which several of the authors on our paper have published on in the recent past. Unfortunately,

length limitations excluded us from addressing this issue in the current work where we chose to focus on the equator-to-pole scale. For the Reviewer's interest, we include a figure analysing the seasonal cycle of atmospheric energy transport across the equator and its changes under external forcing. We note that our analysis focused on the seasonal cycle of cross equatorial energy transport which is an order of magnitude larger than the annual mean hemispheric energy imbalance and has been linked to the width of the tropical precipitation (Donohoe et al., 2019). The changes in transient eddy energy transport (TE) across the equator under $4XCO_2$ appear to be comparable in magnitude to changes in energy transport by the meridional overturning circulation (MOC). We continue to analyse this fascinating result.

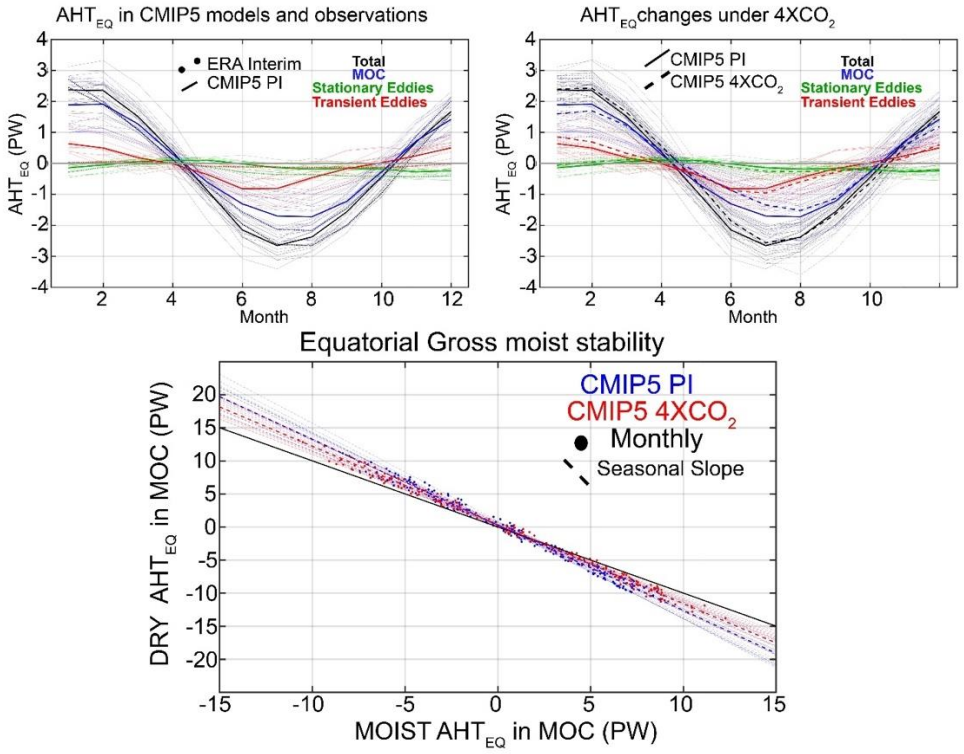


**Figure R3. (Top left) Seasonal cycle of $AHT_{EQ}$ partitioned into transient eddies (red), stationary eddies (green), and MOC in CMIP PI models (solids lines) and reanalysis (dotted lines). (Top right) As in top left but including changes under $4XCO_2$ in CMIP models. (Bottom panel) The dry versus moist $AHT_{EQ}$ in the MOC over the seasonal cycle in PI simulations (blue) and $4XCO_2$ simulations (red).**

7. All figures need to be re-plotted. The biggest problem in all these figures is that the range of y-axis appears to be arbitrary, which is not convenient to the comparison between different subplots. For examples:

a. Fig. 1: Range of y-axis in Fig. 1a can be [-6.0, +6.0], with the 0-line in the middle of the figure. Range of y-axis in Fig. 1b can be [-0.6, +0.6], to be exactly 10% of the Fig. 1a. This will be easier for comparison between the mean value and the changes. Fig. 1c: y-axis, [-200, 100]; Fig. 1d, y-axis, [-20, 10].

Figures 1 now show the y-axis range that you have suggested. Thank you

b. Fig. 2a: y-axis, [-8.0, +8.0]; Fig. 2b: y-axis, [-0.8, +0.8]; Fig. 2d: y-axis, [-200, +100]; Fig. 2e: y-axis, [-20, +10];

Figures 2a, 2b and 2d now show the y-axis ranges you have suggested. Your suggested range for 2e would exclude a substantial number of models and so we have opted to use a range of [-30,+15], which gives a consistent location of the zero axis between panels d and e.

c. Fig. 3a: y-axis, [-6.0, +6.0]; Fig. 3b: y-axis, [-6.0, +6.0].

The Reviewer's suggested y-axis ranges have been implemented for panel 3a. We prefer to have a narrower range of y-axis values for the moisture transport to highlight the correspondence between the residual and high frequency calculations (the point of the figure) in panel b but have symmetrized the positive and negative range from [-4,+4] as suggested by the Reviewer.

d. Fig. 4, for all subplots, please use the same range for y-axis as [-8, +8] for better comparison.

Done.

e. Other figures from Fig. 5 to Fig 10, please adjust y-axis range for a better and easier comparison.

We have revised the y-axis to be symmetric (about zero in all panels) and to reach a compromise for figures that use axes that are consistent across panels and figures that highlight the salient features of each field.

**Cited works:**


Donohoe, A, A.R. Atwood and M.P. Byrne 2019, Controls on the Width of Tropical Precipitation and Its Contraction Under Global Warming, GRL., 46, 9958-9967.

Donohoe, A., and D. Battisti, 2012: What determines meridional heat transport in climate models? J. Climate, 25, 3832–3850.

Liang, M., A. Czaja, R. Graversen, and R. Tailleux, 2018: Poleward energy transport: is the standard definition physically relevant at all time scales? Climate Dyn., 50, 1785–1797

Lucarini, V., and F. Ragone, 2011: Energetics of IPCC4AR4 climate models: energy balance and meridional enthalpy transports. Rev. Geophys., 49, RG1001.

Loeb, N. G., B. A. Wielicki, D. R. Doelling, G. L. Smith, D. F. Keyes, S. Kato, N. Manalo-Smith,
and T. Wong, 2009: Towards optimal closure of the earth's top-of-atmosphere radiation budget. J. Climate, 22, 748–766.

Mayer et el. 2017, *Toward consistent diagnostics of the coupled atmosphere and ocean energy budgets. J. Climate, 30, 9225-9248.*

Trenberth, K. E., and D. P. Stepaniak, 2003b: Seamless poleward atmospheric energy transports and implications for the hadley circulation. J. Climate, 16, 3706–3722.

Wunsch, 2005: *The total meridional heat flux and the oceanic and atmospheric partition, J. Climate, 18, 4374-4380.*

***Forster et al. 2013:*** Evaluating adjusted forcing and model spread for historical and future scenarios in the CMIP5 generation of climate models, JGR Atmospheres, 118, 1139-1150.

%%%%%%%%%%%%%%%%%%%%%%%%%%%%%%%%%%%%

Reviewer 2:

*(i)* I think the authors have overinterpreted Stone's arguments, or at least they present them initially as if they have more general applicability than they in fact do. His arguments are largely based on a one-dimensional energy-balance model, and assume that the meridional heat transport has a very large-scale structure. His results actually say very little about the magnitude of the meridional heat flux. There is certainly no a priori reason that the distribution of TOA radiation should be tightly constrained – it would certainly change if the Earth's rotation rate changed, or if the atmosphere were much thinner, for both would have a large impact on the magnitude of the meridional heat transport and so the net TOA radiation. Even the structure of the heat transport will change if the rotation rate changes sufficiently (admittedly we are not looking at such cases here) or if cloudiness changes significantly. Only the incoming solar radiation is truly constrained by Earth–Sun geometry, and it is the atmosphere's efficiency in heat transport that keeps the TOA radiation more or less constant in the climates that we see or have seen on Earth. The authors do point out later that 'Stone was wrong in the sense. . . ' but that feels like knocking down a straw man.

We thank the Reviewer for these comments that have made us reread and reconsider Stone's arguments. We agree with the Reviewer that our original text overinterpreted Stone's work. Specifically, Stone points out that in the observed climate system, the large-scale gradient of planetary albedo and thermal emission (OLR) have nearly canceling impacts on the MHT and, thus, the magnitude of MHT appears to only depend on Earth-Sun geometry (and global mean planetary albedo). We misinterpreted this argument to apply more generally to speak to changes in TOA radiation and their impact on MHT. We have removed this straw man argument from the revised manuscript.

*(ii)* The above considerations actually make the issue of 'Bjerknes compensation' (where

it does occur) *more* interesting because there has to be a dynamical reason for it – one cannot simply posit that it is a principle based on some rather general considerations. These topics, and some of those in the present manuscript, are discussed more in Farneti and Vallis (JC, 2013), and the results presented here are largely consistent with theirs. For example, the conclusion on P27 that it is adjustments in the atmospheric circulation that smooth the temperature response and keep MHT nearly climate-state invariant is similar to the last sentence of their abstract. The compensation in both cases arises largely because of the transient eddies give rise to an efficient (effectively diffusive or super diffusive) heat transport that compensates for whatever other process is giving rise to a thermodynamic anomaly.

This is a fascinating discussion and we largely agree with the interpretation of the Reviewer (and have added a citation and statement of general agreement with Farneti and Vallis to the revised manuscript). However, there are some components of the argument that "MHT is nearly climate state invariant because of efficient atmospheric dynamics" that continue to perplex us. For example, if the climate is forced at the equator-to-pole scale, an efficient diffusivity suggests the majority of the forcing is balanced by changes in MHT. In the linear one-dimensional framework, the MHT change would be equal to the forcing at the equator-to-pole scales times D/(D+B) where D is the effective diffusivity at the equator-to-pole scale ($6D/a^2$ when cast as a second order Legendre expansion) and B is the linear dependence of OLR on temperature. In physical terms, if the MHT is more efficient than the radiative damping, then the majority of the forcing is balanced by the MHT changes as opposed to radiative feedbacks since the MHT changes can be accomplished with small changes in the temperature gradient. We speculate that some of the simulations analyzed in this work have substantial radiative forcing at the equator-to-pole scale and, thus, the lack of change in MHT is unanticipated under the assumption of efficient dynamics.

Stone (1978) analysis found two regimes in which $MHT_{MAX}$ was insensitive to changes in the effective diffusivity. The first regime is the high efficiency regime in which D is strong enough to nearly flatten the temperature and OLR gradient such that the $MHT_{MAX}$ asymptotically approaches the equator-to-pole ASR gradient (ASR* in the terminology of the present manuscript) as D approaches infinity. Our previous analysis suggest that the observed climate system (and that modeled by GCMs) is not close to this regime; $MHT_{MAX}$ would approach 8.2 (9.0) PW in the NH (SH) in the limit of infinitely efficient dynamics and the observed $MHT_{MAX}$ of 5.3 PW in each hemispheres is about 2/3 of the way toward this limit (Donohoe and Battisti, 2012). Stone's other regime of MHT insensitivity was termed the intermediate efficiency regime whereby an increase in MHT causes a decrease in sea ice. The reduced sea ice decreases the equator-to-pole gradient of planetary albedo which would decrease ASR* and thus be a negative feedback on the initial MHT perturbation. We believe this regime is an artifact of Stone's overemphasis of the contribution of surface albedo changes to the planetary albedo in his one-dimensional model; modern analysis suggest that the meridional gradient of surface albedo only contributes about 0.4 PW to $MHT_{MAX}$ (Donohoe and Battisti, 2012). Therefore, we do not believe the near invariance of the $MHT_{MAX}$ in the

intermediate dynamical efficiency regime applies to the observed system or comprehensively GCMs.

The above points lead to a paradox of how MHT appears to be nearly climate state invariant. We believe the observed system is closer to an intermediate regime where dynamics are more efficient but comparable in magnitude to the efficiency of radiative damping. In this regime, $MHT_{MAX}$ should be sensitive to both external radiative forcing and changes in the effective diffusivity of the system. We have expanded our discussion of these points and how we think the diffusion of moist static energy framework potentially resolves these issues in the revised manuscript's discussion section.

*(iii)* This perspective also provides an explanation for the result that, although the individual models differ from each other in their heat transport, within each model the meridional heat transport varies little. Essentially each model has a different heat diffusivity, although all of them are large. As the climate changes the meridional heat transport in each model is constrained to be fairly constant, but it is constrained to different values in different models. Perhaps this is just another way of expressing what the authors say at the end of their section 7. If so, the authors could make it a bit clearer or if not say why not.

Thanks for this comment. We agree with the Reviewer's statement that models each have a different heat diffusivity but in each the diffusivity is large. However, we believe that the primary reason that models differ in their mean-state MHT is the inter-model differences in the meridional structure of ASR due to differences in cloud radiative effect (Donohoe and Battisti, 2012). This point is best seen from a plot of the inter-model spread (across the preindustrial mean states) of $MHT_{MAX}$ versus ASR* (Figure R3). Since ASR* is either balanced dynamically by $MHT_{MAX}$ or radiatively by OLR*, a crude measure of the efficiency of energy transport (EFF) is the ratio of ASR* to $MHT_{MAX}$. If all models had the same EFF, the individual models would all lie along a single dashed line (lines of efficiency 0.4, 0.5, 0.6 and 0.7 are shown by the dashed lines) and $MHT_{MAX}$ would be determined by ASR* only. If $MHT_{MAX}$ was determined by inter-model differences in EFF, the individual modes would spread across the dashed lines. Figure R4 shows that the models tend to lie within a relatively narrow range of EFF values, and the spread in $MHT_{MAX}$ is primarily determined by ASR* (correlation coefficient of 0.81 in the NH and 0.86 in the SH). In contrast, inter-model difference in EFF are only weakly correlated with $MHT_{MAX}$ (R=0.29 in the NH and 0.19 in the SH) suggesting that inter-model differences in planetary albedo primarily determine $MHT_{MAX}$.

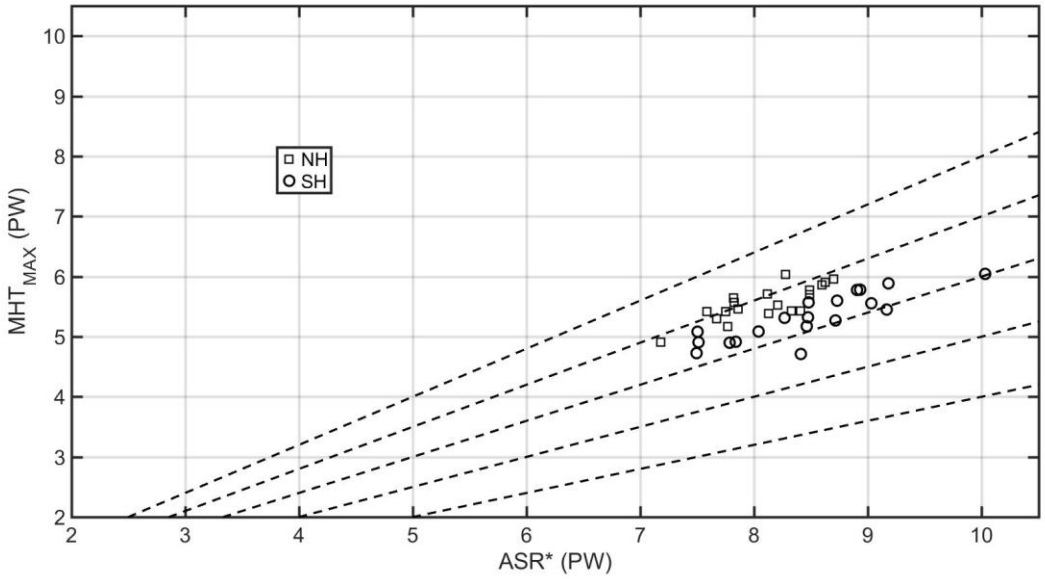


**Figure R4. Inter-model spread of $MHT_{MAX}$ versus ASR* in the CMIP5 preindustrial models. Squares show the Northern Hemisphere (NH) and circles show the Southern Hemisphere (SH) values. Dashed line show constant ratios (0.4,0.5,0.6, 0.7 and 0.8) of $MHT_{MAX}$ to ASR* defined as the heat transport efficiency.**

In response to $4XCO_2$, EFF increases in all models in the NH but does not change robustly in the SH. The inter-model spread in changes in $MHT_{MAX}$ is strongly correlated with changes in ASR* (R =0.86 in NH and 0.92 in the SH) and not significantly correlated with changes in EFF, suggesting that changes in planetary albedo associated with cloud and sea-ice feedbacks determine the inter-model spread in MHT changes more so than changes in dynamical efficiency as was found by Hwang and Frierson (2011).

We have revised and reordered the discussion Section of the revised manuscript and hope that our argument is clearer.

*(iv)* Another study that looks at the variation of heat transport since the LGM and that perhaps deserves reference is that of Yang et al (2005, Scientific Reports), with other papers by the same set of authors addressing related problems.

Thank you for pointing out this reference which we believe was meant to Yang (2015). We have cited this reference and one other by the same set of authors in the revised manuscript. Please see the response to Reviewer 1 major points 3 and 5.

*(v)* A comment is that the authors say (p28) that 'An emerging body of work has argued that, in response to external forcing, atmospheric motions move energy from regions that are inefficient at radiating energy to space to regions that are efficient at radiating energy to space by diffusing moist static energy.' I'd agree with that, but is it harsh to ask what else could happen? Almost any system in which heat is transported from hot to cold will behave in a similar way — a bar of metal that is heated somewhere,

insulated somewhere else but open to air in a third location will do the same.
The twist is the presence of moisture and so the use of moist static energy.
Partitioning between moist and dry energy transport is actually rather interesting.

We agree with the Reviewer that the exact nature of the down-gradient transport rule (e.g. diffusion of temperature versus MSE, the possible spatial structure of the diffusion coefficient, etc.) is unclear given the present literature. In general, a transport rule that moves energy from warm to cool regions in both the climatological and anomalous sense will give qualitatively similar results regarding MHT and its changes. However, previous work by some of the co-authors (Armour et al. 2019) has argued that diffusion of MSE can explain the enhanced AHT under the transient response to increased $CO_2$ in the presence of polar amplified warming whereas diffusion of temperature cannot. Additionally, MSE diffusion has been shown to explain the spatial structure of changes in the hydrological cycle (Siler et al. 2018). Therefore, we believe evidence is beginning to suggest that MSE diffusion has more explanatory power than temperature diffusion.

As the overall climate warms or cools one might expect the partitioning between moist and dry energy transport to be anti-correlated, since moisture can transport more energy in a warmer climate. But if the heat transport is varying because the ocean heat transport is varying, because of some natural variability on decadal timescales for example, then one might expect the moist and dry eddy transports to vary in unison. Is this the case? (The answer may be out of scope, which would be okay.)

Thanks very much for the suggestion. We agree that additional work on the co-variability of moist and dry AHT in response to internal variability versus forced changes would be useful. Below is a preliminary analysis of the spatial temporal structure of the correlation between interannual variability of moist and dry energy transport by the eddies (stationary and transient) for the ERA and NCEP reanalysis. As the Reviewer suspected, the moist and dry transports do vary in unison over the storm track regions of both hemispheres. This result seems consistent between the ERA and NCEP reanalysis. We are hoping to continue analysis of this problem

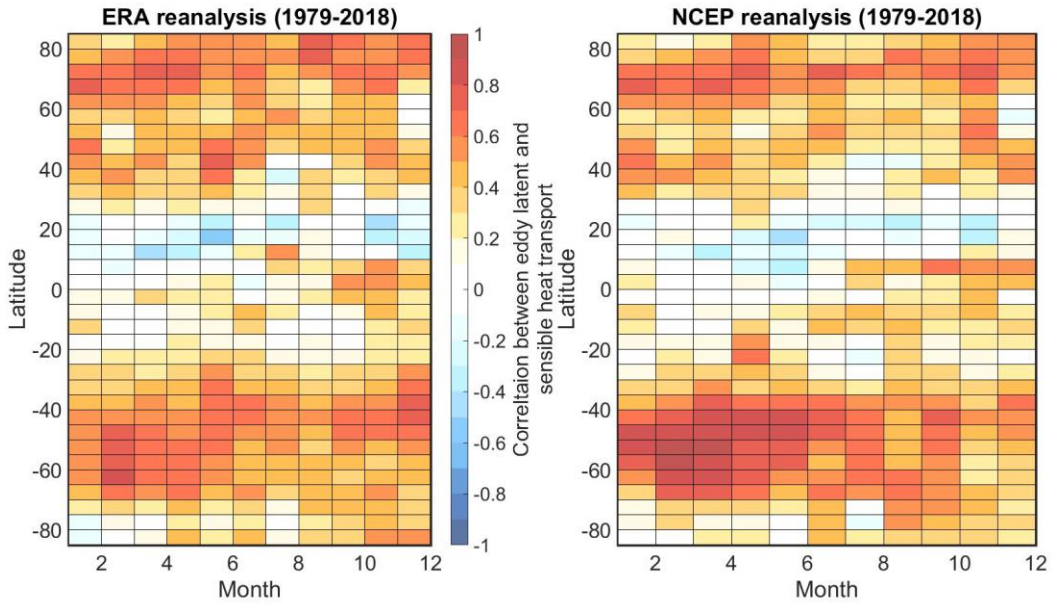


**Figure R5. Correlation between inter-annual variability of moist and dry energy transport by eddies for each latitude and month. Both sets of reanalysis cover the 1979-2018 time period.**

*(vi)* The figures are rather overwhelming, especially Figs 4, 5, 6, 7, 8, 9 and 10, with a total of 66 panels! If the authors feel that all are necessary then I have no objection. But they may wish to consider whether this is the best strategy if they want other people to actually read their paper.

We prefer to keep all the components in these figures as we feel different readers will be interested in different components. We have remade the axes ranges in these figures to make them more approachable. Additionally, the underlying data is available in an online repository should a reader be interested in specific points.

*(vii)* Acronyms are overused. Even when defined (as they mostly are), the use of nonstandard acronyms makes the manuscript hard to follow. OLR, LGM, TOA and GCM are common enough not to cause discomfort, but TE, SE, MHT, AHT, ASR, PI, EBAF. . . ? Heavily acronymed paragraphs (and there are many) become difficult to parse. It would be better to write at least some of them out in full and use acronyms only for the ones that are used most heavily or that will be familiar to most readers.

Thank you for this suggestion. We have written out some of the less well known acronyms in full in selective sentences throughout the revised manuscript to remind the reader of the acronym's meaning. We hope this improves the manuscript's readability.

**Cited works:**

Armour, K., N. Siler, A. Donohoe, and G. Roe, 2019: Meridional atmospheric heat transport constrained by energetics and mediated by large-scale diffusion. J. Climate, 32 (12), 3655– 3680, doi:10.1175/JCLI-D-18-0563.1.

Donohoe, A., and D. Battisti, 2012: What determines meridional heat transport in climate models? J. Climate, 25, 3832–3850.

Farneti, R., and G. Vallis, 2013: Meridional energy transport in the coupled atmosphere-ocean system: compensation and partitioning. J. Climate, 26, 7151–7166.

Hwang, Y., and D. Frierson, 2010: Increasing atmospheric poleward energy transport with global warming. Geophys. Res. Lett., 37, L24 807.

Siler, N , G.H Roe and K.C. Armour . 2018: Insights into the zonal-mean response of the hydrologic cycle to global warming from a diffusive energy balance model, J. Climate, 31, 7481-7493

Stone, P., 1978: Constraints on dynamical transports of energy on a spherical planet. Dynam. Atmos. Oceans, 2, 123–139.

Yang, H., Y. Zhao, Q. Li, and Z. Liu, 2015: Heat transport in atmosphere and ocean over the past 22,000 years. Nature Scientific Reports, 5: 16661.

%%%%%%%%%%%%%%

Reviewer #3: This manuscript diagnoses the energy transports in CMIP5 GCMs in preindustrial, 4xCO2, and Last Glacial Maximum simulations and compares the PI results to those inferred from two reanalysis products. The claim of a novel technique for the energy transport calculations was intriguing but ultimately unfounded; all of the methods are pretty much standard in the literature. And there were other important problems with the methodology and how it is presented. The actual results seem reasonable overall, but I'm not sure if they're especially important. As such, major revisions are necessary.

Major comments

1. What is novel about these calculations?

The abstract and introduction refer to a ``novel'' technique to infer the transient eddy terms using monthly mean data. But the technique ultimately used, namely inferring the transient term as a residual from the boundary fluxes and the time-mean terms, is well established. See e.g. [hill_mechanisms_2015,xiang_contrasting_2018,rencurrel_exploring_2018,rencurrel_efficiency_2019], and almost surely others. Is there some detail about the calculation that I've missed? If not, this phrasing is inappropriate. I suppose it's possible that no prior studies have shown an explicit validation of the eddies-as-residual calculation against the explicit calculation. So that's useful. But the fact that it works is not exactly surprising.

This eddies-as-residual calculation is also a particular case of a broader methodology that the authors use elsewhere ubiquitously: given two terms that are constrained to sum up to a third term, and if term two and term three are known, then term one can be inferred by subtracting term two from term three. The authors make use of this extensively for the partitioning of total energy transport between the atmosphere and ocean and of the atmospheric energy transport between dry static energy and moisture components. As have many previous studies. Further reason that the "novel" framing is problematic.

Thank you for pointing out these previous studies that have used a conceptually similar methodology for backing out the transient eddy transports as a residual within a single GCM. We agree with the Reviewer that our previous claim of a “novel” technique is unjustified and have removed these statements from the abstract and text of the revised manuscript. We have also added citations to previous studies which have used this conceptual technique within a single model.

We do, however, emphasize that the current work is the first study (to our knowledge) to diagnose changes in the partitioning of MHT consistently across an ensemble of climate model simulations. Additionally, our technique differs from previous studies in the treatment of the mass budget used to calculate the MOC AHT and also in the calculation of the atmospheric energy tendency (with respect to a fixed atmospheric pressure). We believe it is important to document the specifics of these calculations for replicability purposes, especially given how well our technique reproduces the transient

eddy energy and moisture fluxes produced from the direct (high temporal frequency) model output in CESM (Section 2c).

2. Methodology could be more succinct and better organized

This relates to the preceding comment. The diagnostics being presented --- inferred total transports from TOA and surface fluxes, partitioning into mean vs. eddy terms and moisture vs. DSE terms, are all pretty much standard in the literature. But they are described in a confusing order and, I believe as a result, in places in excessive detail.

For example, the first equation presents MHT not as the sum of OHT and AHT but as the sum of OHT and the atmospheric mean and eddy components. Then Eq. 2 switches focus to MHT as due to the net TOA radiative flux, and then Eq. 3 jumps back to the calculation of AHT as the sum of mean and eddy terms. Subsection 2b is then quite repetitive of things from 2a, in particular lines 239-241, 265-267, and 268-276.

An alternative organization for the authors to consider would be: explain all of the transports from a theoretical perspective first, followed in a separate sub-section by the details of how they are actually computed in the models and reanalyses. And within the energy transports description, start with the MHT, then its partitioning into OHT and AHT (and the neglected storage terms), then the partitioning of AHT into the mean and eddy terms, and then the partitioning of the atmospheric terms into dry vs. moist components.

We thank the Reviewer for the thoughtful suggestion of reorganizing the discussion. However, we prefer the organization of the methods section as written; it is the result of many drafts and much discussion amongst the co-authors on how to structure the methods to so they are in line with the order the results are presented. The switching between the dynamics and radiative perspectives in the first three equations is intentional and is meant to give the reader an appreciation of the different pieces of information and quantities used to dissect MHT in the presentation of results (Section 3) and in the discussion. The first equation is essentially the equation suggested by the Reviewer (MHT = AHT+OHT, note the underbrace in that equation) but additionally broken down into the atmospheric components. We elected not to present Eq. 1 this as two separate equations to make the presentation succinct. Eq. 1 as written represents the thrust of our work as we focus on the atmospheric partitioning and do not further decompose the OHT. Thereafter, the presentation in the discussion is ordered by the conceptual methodology used to partition MHT from observations followed by the conceptual methodology used to partition MHT in models. Although the same quantities are discussed in both of these subsections, the details of how the terms are calculated differ and are important to document.

3. Neglected annual-mean heat storage during initial, transient century

The 4xCO2 results are averages over years 50-100; the LGM results are averages over

``the last 50 years of the simulations," but I didn't see the simulation length anywhere. So this may or may not be relevant for the LGM, but it certainly is for the 4xCO2: atmospheric energy transports, ocean heat uptake patterns, and ocean heat transports evolve throughout the first, transient century after an imposed forcing. This means that the equilibrium responses may differ materially from those inferred in the initial century, and more importantly that annual-mean heat storage changes (particularly for the ocean) can be nontrivial and need to be accounted for when computing energy transports. See in particular [he_transient_2019].

This issue was explicitly addressed in the original (and revised) manuscript, specifically in regard to the disequilibrium under $4XCO_2$ (excerpts pasted below):

downwelling and upwelling radiation at the surface. We note that Eq. 4 is valid when the ocean is in *equilibrium*. When the system is not in equilibrium (i.e. the ocean is accumulating energy), Eq. 4 expresses the *implied* OHT which is the sum of OHT and the spatial integral of the tendency in ocean heat content. Thus, our comparison of OHT diagnosed from Eq. 4 in the PI and LGM (equilibrium) simulations versus the $4\times CO_2$ (transient) simulations do *not* constrain changes in OHT since the latter includes the impact of transient ocean storage. However, the change in AHT

and

From a dynamics perspective there is a robust increase in poleward AHT under $4\times CO_2$ (Fig. 2b) in both hemispheres (Hwang and Frierson 2010) with nearly compensating decreases in implied poleward OHT (see Fig. 11B in Held and Soden 2006). The changes in implied OHT are due to the spatial pattern of transient ocean heat uptake that preferentially occurs in the high latitude oceans (Marshall et al. 2015; Armour et al. 2016). We can visualize the degree of compensation

In the revised manuscript, we also remind the reader that:

"It is unclear whether the increase in poleward AHT and decrease in implied OHT under $4XCO_2$ would also be a feature of the fully equilibrated $4XCO_2$ climate (Chengfei, 2019)."

4. Comparing pre-industrial simulations to present-day obs

Strictly speaking the comparison between the models and observations+reanalyses is apples to oranges: the models are preindustrial, the obs/reanalyses are present-day. As such, the difference between them cannot be unambiguously claimed to be due to model bias. That would require analysis of the CMIP5 historical simulations, averaged over the

same time period as used for the obs+reanalyses. (To be fair, I don't expect this to make a huge difference.)

Thank you for raising this point. We chose to use the PI simulations because we wanted an equilibrium climate state to allow a calculation of the role of ocean heat transport without the complication of transient heat uptake. We agree with the Reviewer that this complicates the comparison with observations. Below, we show the AHT and OHT at the latitude of $MHT_{MAX}$ in the pre-industrial (black) and historic simulations (red) akin to Fig. 2c of the manuscript. The "historic" simulations are averaged from 2000-2016 to correspond to the observational analysis and only the subset of models that have the necessary model output for historical simulations are included. Solid black lines connect the PI and historical values calculated from the same model. Overall, there is very little mean model difference in the $MHT_{MAX}$ between the PI and historical simulations (ensemble mean difference < 0.04 PW in both hemispheres) and the mean absolute difference in $MHT_{MAX}$ is also fairly small (0.06 PW in the NH and 0.03 in the SH) with no single model difference exceeding 0.11 PW. Interestingly, the ensemble average implied poleward OHT in the SH is reduced by 0.10 PW in the historic period compared to pre-industrial, and the AHT is greater by nearly the same amount. We speculate that this results from transient heat uptake in the Southern Ocean in response to historical forcing. In the NH, differences in AHT and OHT between the preindustrial and historic period are less uniform between models and have a small mean absolute value <0.07 PW (the NORESM is an exception; in that model, AHT and OHT change by 0.6PW in opposite directions). We have added a brief discussion of these points to the Section 4 of the revised manuscript.

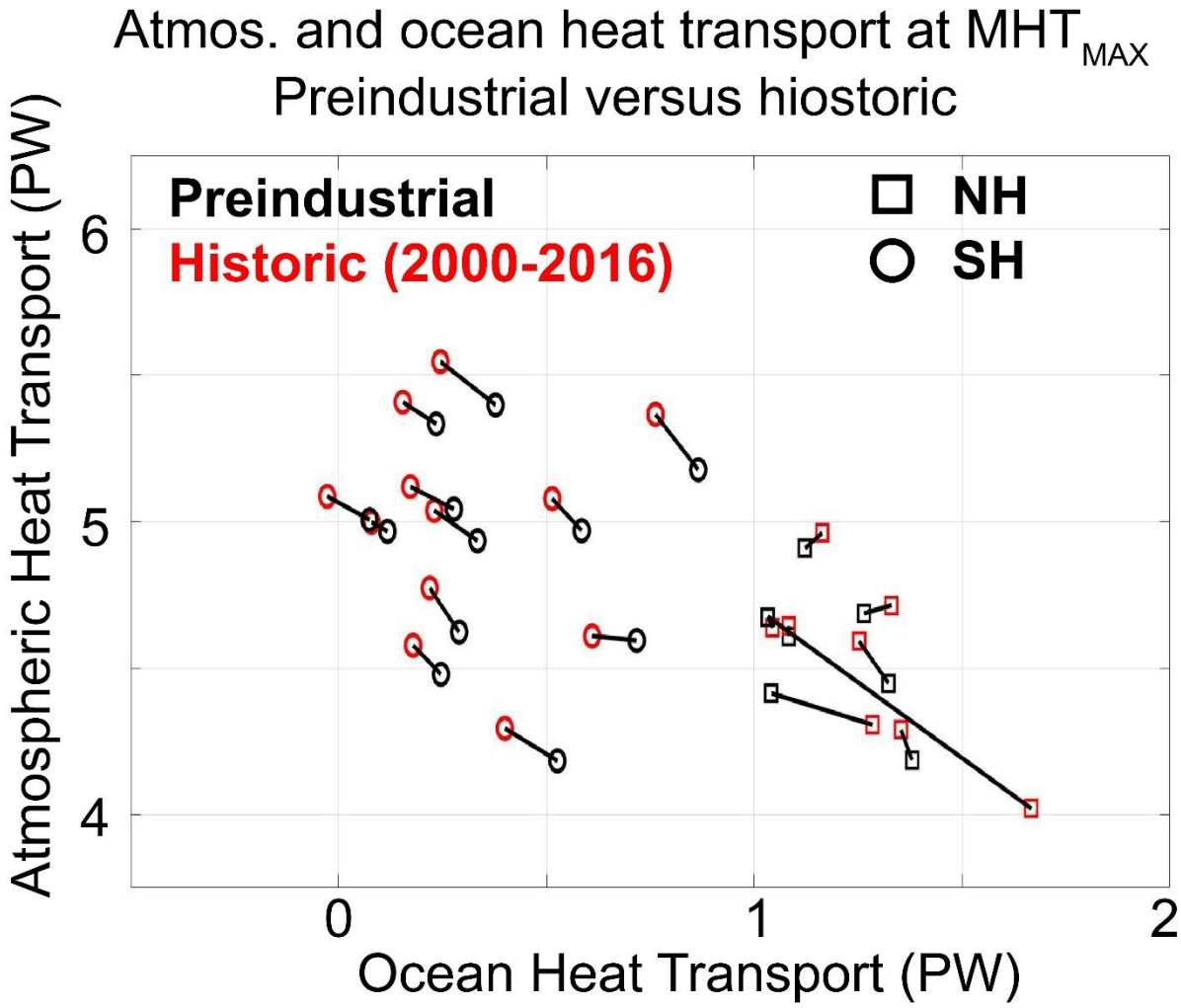


**Figure R6. Atmosphere and Ocean energy transport contributions at the latitude of $MHT_{MAX}$ in the historic period (red, averaged from 2000-2016) and in the preindustrial simulation (black). Squares are for the Northern Hemisphere and circles show the Southern Hemisphere values. The lines connect values from the same climate model.**

5. Different set of models for 4xCO2 and LGM simulations

From Tables 1 and 2, the models used for the LGM calculations is not a proper subset of the 4xCO2 models. To bolster the credibility of the claims about differences between the responses to either perturbation more, the manuscript should present somewhere a discussion of the results averaged over that subset of models (if I'm reading the tables correctly, CCSM4, CNRM CM5, MPI ESM P, and MRI CGCM3) that performed both simulations.

The reviewer is correct: output was not available for us to calculate all the energy transport terms for all three climate states (LGM, PI and $4XCO_2$) from seven CMIP5 models (listed in Table 2). [We inadvertently left MIROC ESM, GISS E2R and MPI ESM LR off of Table 1 in the original manuscript (a previous set of analysis did not include $4XCO_2$ simulations for these models but they are included in the manuscript plots).] Figures 1 and 2 include only results from these seven. This information has been added to the revised figure caption.

To test the robustness of the $4XCO_2$ changes to the subset of models used, we show below in Figs. R7 and R8 the ensemble average $4XCO_2$ changes in all 20 models used for the $4XCO_2$ analysis (solid lines) and the subset of seven models that have LGM simulations (dashed lines). These figures demonstrate that the $4XCO_2$ changes in MHT, AHT, OHT and the partitioning of the AHT into SE, MOC, and TE are robust across the subset of models used for the LGM.

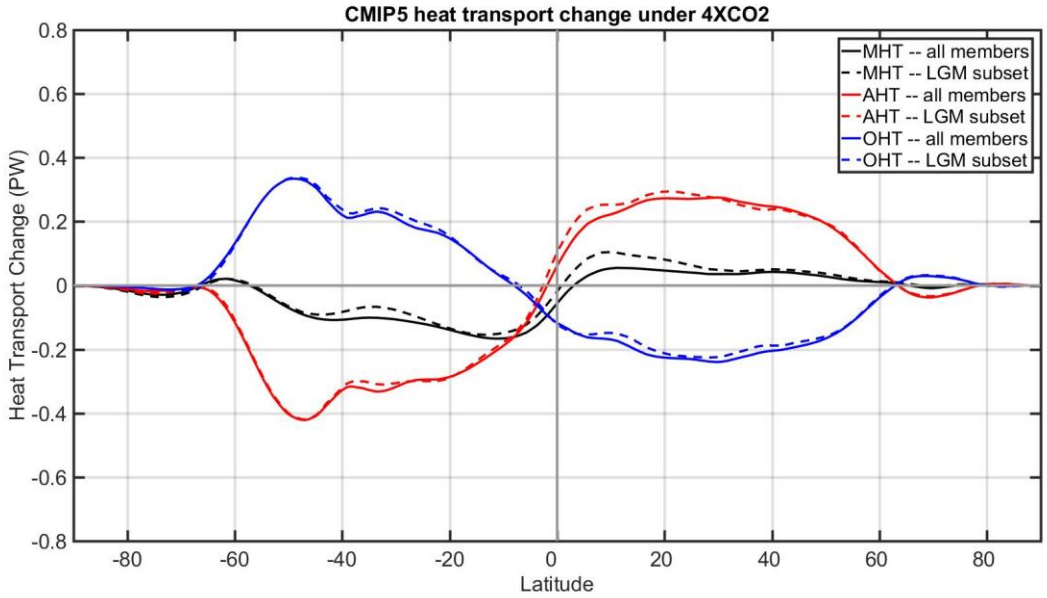


**Figure R7. Ensemble mean change in MHT (black), AHT (red) and OHT (blue) under $4XCO_2$ in all CMIP5 models with $4XCO_2$ simulation (solid) and the subset of seven models with LGM simulations (dashed).**

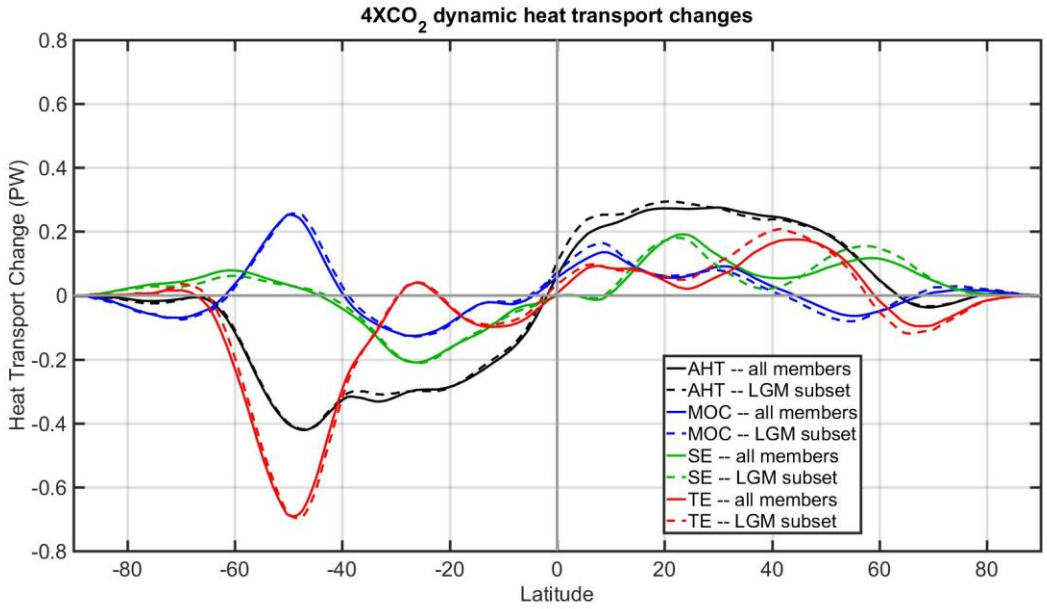


**Figure R8. Ensemble mean change in AHT (black) subdivided into changes in MOC (blue), stationary eddies (SE, blue) and transient eddies (TE, red) under $4XCO_2$. The solid line shows the ensemble mean of all CMIP5 models with $4XCO_2$ simulation and the dashed line of the ensemble mean of the subset of seven models with LGM simulations.**

Minor comments
==========

- Section 1: The introduction jumps back and forth between results

We introduce a single result (the near invariance of MHT) in the introduction in addition to a summary of pertinent literature to frame the research questions. We would be more than happy to address specific concerns the Reviewer may have in our presentation.

- 70: "participating the"

Changed to “participating in the”.

- 73-76: This makes it sound like it is one contiguous simulation spanning LGM to PI to 4xCO2

Rewritten to indicate these are separate climate simulations.

- 90: "lion's share" is too colloquial for an academic paper in my opinion. Likewise for "eye-catching" on line 508.

Eye-catching has been changes to “striking” in the revised manuscript. We believe “lion’s share” as defined in Miriam Webster dictionary is appropriate wording for the intended meaning here.

- 114: "letent"

Fixed.

- 113-115: Phrasing is a bit imprecise, because in the Tropics the poleward sensible heat transport anomaly wins out over the equatorward latent heat transport anomaly, whereas in the mid-latitudes the poleward latent heat transport anomaly wins out over the equatorward sensible heat transport anomaly

Changed to “changes in latent heat transport are opposed by changes in sensible heat transport in both regions, resulting in a modest change in total AHT.

- 164-165: It should be made clear that whether AHT or OHT is the "residual" is arbitrary: one could compute the implied AHT from the sum of the TOA and surface fluxes, and compute OHT as MHT minus AHT. (In fact, one could just as well compute AHT and OHT directly and then add them to "infer" MHT.)

Rewritten to say that AHT is calculated from the difference between TOA and surface fluxes.

- 183: Earth's

Fixed.

- 192: Strictly speaking, Eq. 2 doesn't include the subtraction of the global mean, unless the ASR and OLR terms are taken to be the local anomalies from the global mean.

This point is discussed in text following the equation. We prefer to keep the equation compact and discuss the correction in the text.

- 222: Even if they are the dominant contributor to the eddy flux, it's incorrect to refer to the transient term solely as due to baroclinic eddies.

Agree. We have changed this to read: “that is primarily associated with baroclinic synoptic eddies”.

- 297-299: Note that the interpolation from the model-native vertical coordinates to regular pressure levels can introduce budget residuals, although for these zonal-mean transports it doesn't appear to be a large term.

Noted in the revised manuscript: “We note that the output is interpolated to pressure levels from the model's native vertical coordinate akin to the CMIP archived data. This choice was made to test if the interpolation introduces energy budget residuals.”

- 577-579 vs. 591-592: These feel contradictory: the first makes the case that the local TOA radiative response can be large, invalidating Stone's appeal to a fixed overall pattern, and the second says that that overall meridional pattern is, indeed, modestly changed.

The distinction is that the local net radiation can change substantially, but that the changes at the equator-to-pole scale are modest. We have rewritten the former sentence to clarify that this statement refers to local radiative changes. We have also backed off on our criticism of Stone (1978) following the suggestions of Reviewer 2.

- 654: [held_nonlinear_1980], not Held 1980.

Fixed.

- 682: "he"

Fixed.

- 695: At first glance, the footnote "2" looks like the storage term is being raised to the second power.

Footnote moved to the next sentence to avoid confusion.

- Figures: Zonally integrated energy transports incorporate the local surface area at each latitude and its decrease moving poleward. So it's unnecessary (and potentially misleading) to plot them vs. sin(latitude) rather than simply latitude.

Thank you for the comment. Figures 1 and 2 use an abscissa of sin(latitude) while the remainder of the figures use latitude. This choice was made because these figures, and the accompanying text in the manuscript, relate the TOA radiation and its changes to the total meridional heat transport. The net radiation needs to be spatially weighted to make this comparison and we prefer to use the same abscissa in the panels of this figure

showing the resultant energy transports (upper panels) for consistency and ease of comparison.

## Cited works

Chengfei, H., Z. Liuand, and A. Hu, 2019: The transient response of atmospheric and oceanic heat transports to anthropogenic warming. Nature Climate Change, (222), doi:10.1038/s41558-018-0387-3.

Track Changes Version of the revised manuscript

# The partitioning of meridional heat transport from the Last Glacial Maximum to $CO_2$ quadrupling in coupled climate models

Aaron Donohoe*

*Polar Science Center, Applied Physics Lab, University of Washington, Seattle, WA, USA*

Kyle C. Armour

*School of Oceanography and Department of Atmospheric Sciences, University of Washington, Seattle, WA, USA*

Gerard H. Roe

*Department of Earth and Space Sciences, University of Washington, University of Washington, Seattle, WA, USA*

David S. Battisti

*Department of Atmospheric Sciences, University of Washington, Seattle, WA, USA*

Lily Hahn

*Department of Atmospheric Sciences, University of Washington, Seattle, WA, USA*

*Corresponding author address:* Applied Physics Lab, University of Washington, 1013 40th street, Seattle, Washington/USA.

E-mail: adonohoe@u.washington.edu

ABSTRACT

Meridional heat transport (MHT) is analyzed in ensembles of coupled climate models simulating climate states ranging from the Last Glacial Maximum (LGM) to quadrupled $CO_2$. MHT is partitioned here into atmospheric (AHT) and implied oceanic (OHT) heat transports. In turn, AHT is partitioned into dry and moist energy transport by the meridional overturning circulation (MOC), transient eddy energy transport (TE) and stationary eddy energy transport (SE) using only monthly averaged model output that is typically archived. In all climate models examined, the maximum total MHT (AHT+OHT) is nearly climate-state invariant, except for a modest (4%, 0.3PW) enhancement of MHT in the Northern Hemisphere (NH) during the LGM. However, the partitioning of MHT depends markedly on the climate state and the changes in partitioning differs considerably among different climate models. In response to $CO_2$ quadrupling, poleward implied OHT decreases while AHT increases by a nearly compensating amount. The increase in annual-mean AHT is a smooth function of latitude but is due to a spatially inhomogeneous blend of changes in SE and TE which vary by season. During the LGM, the increase in wintertime SE transport in the NH mid-latitudes exceeds the decrease in TE resulting in enhanced total AHT. Total AHT changes in the SH are not significant. These results suggest that the net top of atmosphere radiative constraints on total MHT are relatively invariant to climate forcing due to nearly compensating changes in absorbed solar radiation and outgoing longwave radiation. However, the partitioning of MHT depends on detailed regional and seasonal factors.

## 1. Introduction

The total (ocean plus atmosphere) meridional heat transport (MHT) across a latitude circle by the coupled (ocean-atmosphere) climate system must, on long timescales, be balanced by the net top of atmosphere (TOA) radiative deficit spatially integrated over the polar cap bounded by a latitude circle (e.g. Vonder Haar and Oort 1973). This constraint offers two conceptually different but numerically equivalent frameworks for diagnosing and analyzing MHT. In a *dynamic* framework, MHT is equal to the vertically and zonally integrated net transport of energy across the latitude circle by atmospheric and oceanic motions due to the contrasts in energy content of equatorward and poleward flowing air/water (Lorenz 1953; Oort 1971). In an *energetic* framework, MHT is equal to the net TOA radiative deficit integrated over the extratropics or, equivalently, the net radiative excess integrated over the tropics. The hemispheric scale radiative imbalance results from the equator-to-pole gradient of absorbed solar radiation (ASR) being steeper than that of outgoing longwave radiation (OLR, Trenberth and Stepaniak 2004; Oort and Haar 1976).

In a seminal paper, Stone (1978) argued that the observed maximum poleward MHT in each hemisphere ($\mathrm{MHT}_{MAX}$) is primarily dictated by Earth-Sun geometry and relatively insensitive to the details of the atmospheric state due to nearly canceling contributions of the equator-to-pole gradient in planetary albedo and OLR. More recent work has demonstrated that the large-scale distribution of net TOA radiation can vary substantially between different climate models because cloud properties fundamentally control the ASR distribution (Donohoe and Battisti 2011) but have a modest impact on OLR. As a result, $\mathrm{MHT}_{MAX}$ differs by as much as 20% between different climate models in simulations of the pre-industrial climate due to differences in cloud distributions/properties (Donohoe and Battisti 2012). However, several studies have demonstrated that *within a single model* $\mathrm{MHT}_{MAX}$ is nearly invariant to the state of the oceanic circulation (Far-

neti and Vallis 2013; Enderton and Marshall 2009), in the interannual variability (Vellinga and Wu 2008) and across paleoclimate states (Yang et al. 2015b). These results raise two key questions. First, how does MHT and its partitioning vary across climate states within ensembles of comprehensive, coupled global climate models (GCMs), given that clouds (and other forcings and feedbacks) can cause substantial changes in net TOA radiation? Second, what dynamical processes in the atmosphere and ocean contribute the MHT changes under climate forcing?

Here we consider MHT and its changes as simulated by an ensemble of comprehensive climate models participating in the Coupled Model Intercomparison Project phase 5(CMIP5; Taylor et al. 2012). We examine MHT within three different climate states: the climate at the Last Glacial Maximum (LGM), the climate under pre-industrial (PI) $CO_2$ conditions, and the climate with $CO_2$ levels set at four times the pre-industrial concentration ($4\times CO_2$). Earth's simulated global-mean surface temperature differs by approximately 10°C between the LGM simulations and the end of the 150-year long $4\times CO_2$ simulations owing to the substantial increase in $CO_2$ and the elimination of large Northern Hemisphere ice sheets. Nonetheless, the ensemble average $\mathrm{MHT}_{MAX}$ is nearly invariant between the simulated LGM, PI and $4\times CO_2$ climate states (Fig. 1A) changing by only 4% in the Northern Hemisphere (NH) and by only 2% in the Southern Hemisphere (SH). This result suggests that while cloud properties and their changes play an important role for the inter-model spread of $\mathrm{MHT}_{MAX}$ in climate models when forced by identical (pre-industrial) forcings (Donohoe and Battisti 2012), the large-scale distribution of net TOA radiation, and thus MHT, is nearly invariant over a wide range of climate states (Fig. 1), just as Stone (1978) speculated.

The smooth, monotonic decrease in both (annual-mean) ASR and OLR from the equator to pole mandates that MHT be a smooth and continuous function of latitude peaking in magnitude in the mid-latitudes of each hemisphere (Trenberth and Stepaniak 2003b). Yet the atmospheric and oceanic circulations that accomplish the total MHT have a rich spatial structure (Trenberth and

Caron 2001; Armour et al. 2019). In the deep tropics the atmosphere and ocean make comparable contributions to MHT (Fig. 2A), each dominated by the mass-overturning circulation in the atmospheric Hadley cells and wind-driven oceanic cells respectively (Held 2001). In the extratropics (poleward of 30° latitude) the atmosphere does the lion's share of the MHT and is comprised of the following transport processes: (i) transient eddies which dominate energy transport in the mid-latitude with latent- and sensible-heat transports that peak on the equatorward and poleward side of the storm track, respectively; (ii) stationary eddies in the subtropics associated with monsoons that transport latent heat during the summer in both hemispheres and, (iii) orographically and diabatically (i.e. land-ocean contrast) forced stationary eddies in the NH winter that transport sensible heat polewards on the poleward flank of the storm track (Fig. 3; Masuda 1988).

How do these different circulations adjust to produce a nearly-invariant and meridionally-smooth pattern of MHT across radically different climate states? Previous studies point to compensating changes in the various components that comprise total MHT:

- *Oceanic and atmospheric energy transports.* If TOA radiation is climate-state invariant, changes in meridional (implied) oceanic heat transport (OHT) must be compensated by changes in meridional atmospheric heat transport (AHT), as originally proposed by Bjerknes (1964). This principle has been demonstrated using idealized models in which ocean basin geometry (Enderton and Marshall 2009) and the planetary rotation rates (Vallis and Farneti 2009) are changed; in both cases, distinct changes occurred in ocean circulations and OHT but MHT (= OHT + AHT) remained nearly unchanged due to compensating AHT changes. In other modeling studies, the compensation between OHT and AHT is imperfect (i.e. MHT changes) due to large changes in sea-ice cover (Enderton and Marshall 2009) or in cloud cover (Liu et al. 2018a) such that changes in ASR are not balanced by those in OLR.

- *Latent and sensible energy transport in the atmosphere.* In response to global warming, the moistening of the atmosphere results in an increase in moisture transport (Held and Soden 2006) in both the deep tropics (equatorward transport in the surface branch of the Hadley cell) and mid-latitudes (poleward transient eddy transport). Climate models show that changes in latent heat transport are opposed by changes in sensible heat transport in both regions, resulting in a modest change in total AHT (Hwang and Frierson 2010; Armour et al. 2019).

- *Transient and stationary eddy transports in the atmosphere.* Model simulations suggest that in response to the enhanced topography of the Laurentide ice sheet during the LGM, AHT by atmospheric stationary eddies increases (Li and Battisti 2008) but that transient eddy AHT simultaneously decreases, despite the enhanced meridional temperature gradient (Donohoe and Battisti 2009), leaving AHT and total MHT nearly unchanged.

Despite these compensation mechanisms, it is not clear why the equator-to-pole gradient in net TOA radiation is so constant as to produce nearly invariant MHT over a wide range of climates. Additionally, it is not clear why total MHT remains invariant when there are large changes in the mix of processes responsible for AHT (Trenberth and Stepaniak 2003a; Armour et al. 2019).

Traditionally, the partitioning of AHT requires that the transient eddy energy transport be calculated from high temporal resolution (i.e. six hourly) data – a computationally expensive calculation to perform across an ensemble of models. For this reason, the change in AHT partitioning under climate forcing has been diagnosed in single model studies (Wu et al. 2011; Enderton and Marshall 2009; Yang et al. 2015a) but not across a full ensemble of models. Changes in AHT due to increased $CO_2$ differ substantially across climate models due to the inter-model spread in the spatial structure of cloud feedbacks and ocean heat uptake (Trenberth and Fasullo 2010; Hwang and Frierson 2010; Hwang et al. 2011; Zelinka and Hartmann 2012; Frierson and Hwang 2012;

Huang and Zhang 2014; Armour et al. 2019). Therefore, AHT changes identified within a single model might not isolate robust physical mechanisms from those contingent on the specific cloud parametrization within a single model.

The primary goal of this work is to partition the mean state and forced changes in MHT in large ensembles of coupled GCMs in order to identify (i) model biases in the mix of processes contributing to total MHT and (ii) changes in the partitioning of MHT in response to climate forcing that are robust across the models. We describe a methodology that allows AHT to be partitioned into different circulations (overturning, stationary eddies, transient eddies) and thermodynamic (latent, sensible, potential) contributions from standard monthly mean climate model output. Conceptually similar methodologies have been used in single model studies (Hill et al. 2015; Xiang et al. 2018; Rencurrell and Rose 2018; Rencurrel and Rose 2020). Here, we apply this methodology across 20 different CMIP5 GCMs to consistently partitioning AHT and diagnose robust features and changes between LGM, pre-industrial, and $4\times CO_2$ climates.

This manuscript is organized as follows. In Section 2a we discuss the calculation of MHT partitioning in the modern climate using satellite data and reanalysis products. In Section 2b we introduce the methodology for partitioning AHT in climate models using monthly mean output and in Section 2c we demonstrate the accuracy of this method using high temporal output from a climate model. In Section 3, we provide an overview of the results, focusing on the near-invariance of total MHT from the LGM to $4\times CO_2$ and how this result is achieved from dynamical and radiative perspectives. In Section 4, we compare the MHT partitioning in climate models to the observational estimates. In Sections 5 and 6, we analyze the simulated MHT partitioning changes under $4\times CO_2$ and LGM conditions, respectively. A summary and conclusion follows.

## 2. Data and methods

We partition MHT into OHT and AHT components, and further decompose AHT into meridional overturning circulation (MOC), stationary eddy (SE) and transient eddy (TE) contributions:

$$\mathrm{MHT} = \mathrm{OHT} + \underbrace{\mathrm{MOC} + \mathrm{SE} + \mathrm{TE}}_{\mathrm{AHT}}. \quad (1)$$

Our method partitions the MHT and the various components of AHT based on standard *monthly mean* climate model output whereas the observed AHT is calculated directly from high temporal resolution three-dimensional atmospheric reanalysis products:

- *Observations:* We calculate the vertically and zonally integrated atmospheric energy transports ($\equiv$ AHT) from two different high temporal (6-hourly) and spatial resolution reanalysis products (see below) that permit an explicit calculation of the TE contribution. Total MHT is calculated from satellite TOA radiation and the OHT is diagnosed as a residual as in Trenberth and Caron (2001).

- *Models:* We diagnose the total MHT from monthly mean TOA radiation, the implied OHT from the monthly mean surface energy fluxes and AHT from the difference between TOA and surface energy fluxes. We then calculate the AHT associated with the time invariant meridional overturning circulations and stationary eddies (MOC and SE) from monthly mean model output and diagnose the TE contribution as a residual.

The observational and model approaches differ because of the contrasting reliability and availability of model and observational data. Observationally based surface energy fluxes are not reliable at the global scale whereas they are standard output from climate models. The direct calculation of three dimensional transient eddy energy transports that we use in the observations requires six-hourly atmospheric data which is readily available in reanalysis data, but is not usually output in

climate model simulations because of the enormous storage requirements. The details of these approaches are outlined below.

*a. Partitioning of MHT, AHT and OHT in observations*

We begin by discussing the calculation of annual mean oceanic and energy transports in an equilibrium climate state with no energy tendency (storage) in the atmosphere or ocean – thus providing the constraint of energy balance in the atmosphere and ocean. The total MHT at any latitude is equal to the energy transport required to balance the TOA radiative imbalance spatially integrated over the polar cap bounded by that latitude:

$$\mathrm{MHT}(\theta) = -2\pi a^2 \int_{\theta}^{90} \cos(\Theta)\,[\mathrm{ASR}(\Theta) - \mathrm{OLR}(\Theta)]\,d\Theta, \tag{2}$$

where $a$ is the radius of Earth, $\theta$ is latitude, and the cosine in the integrand accounts for spherical geometry. TOA radiation data is taken from the climatology of the Clouds and Earths Radiant Energy Systems (Wielicki et al. 1996) Energy Balance and Filled product (Loeb et al. 2009) version 4.0 from March of 2000 to December 2016. In theory, global-mean energy balance ensures that MHT($\theta$) is independent of whether the TOA radiative imbalances are integrated from $\theta$ to the North Pole (as written in Eq. 2) or from the South Pole to $\theta$ (with negative sign omitted). In practice, there is a non-zero global-mean value of (ASR-OLR) that must be subtracted from the integrand above to ensure that MHT goes to zero at both poles; we assume this energy imbalance is spatially invariant and thus subtract a constant value at all latitudes, but note this as an important caveat to the calculation of climatological MHT in both observations and models. For the CERES EBAF data, the global radiative imbalance is equal to the long-term ocean heat uptake calculated from ARGO data of +0.65 W m$^{-2}$ (Johnson et al. 2009). We use this same approach (i.e. Eq. 2) to calculate MHT in coupled climate models where the ensemble mean absolute values of global

mean TOA net radiative imbalance in PI models is $\approx 0.5$ W m$^{-2}$ TOLucarini and Ragone ((similar that in CMIP3 models 2011) which translates to a $\pm 0.1$ PW adjustment of MHT$_{MAX}$. Energy imbalance in the PI control simulations could arise from either not reaching full equilibration or from a lack of energy conservation, primarily within the atmospheric model component (Hobbs et al. 2016). Because energy non-conservation appears to be largely invariant over time and across forcing scenarios of CMIP5 models (Hobbs et al. 2016), we expect the calculation of heat transport changes to be largely unaffected by this issue.

We calculate the AHT as the vertically (mass-weighted) and zonally-integrated meridional transport of moist static energy, MSE $= c_p T + Lq + gZ$ where $T$ is the atmospheric temperature, $c_p$ is the specific heat of air at constant pressure, $L$ is the latent heat of vaporization of water, $q$ is the specific humidity, $g$ is the acceleration of gravity, and $Z$ in the geopotential height. We use two different atmospheric reanalyses products for our calculations: (i) the NCEP reanalysis product (Kalnay et al. 1996), which has a horizontal spectral resolution of T62 and 17 vertical levels, and (ii) the ERA interim reanalysis product (Dee et al. 2011), which has a horizontal resolution of 1.5° and 37 vertical levels. We use 6-hourly fields to calculate the energy transport for each month over the 2000-2016 time period, averaging the results over all years to define the climatological AHT (for each month). The velocities and MSE are subdivided into the zonal and time mean, transient eddy, and stationary eddy components (as in Priestley 1948; Lorenz 1953). In this framework, the vertically and zonally integrated total energy transport is:

$$\mathrm{AHT}(\theta) = \frac{2\pi a \cos(\theta)}{g} \int_0^{P_s} \underbrace{[\bar{V}]\,[\overline{\mathrm{MSE}}]}_{\mathrm{MOC}} + \underbrace{[V^* \mathrm{MSE}^*]}_{\mathrm{SE}} + \underbrace{\overbrace{\left[\overline{V^{*\prime} \mathrm{MSE}^{*\prime}}\right]}^{\mathrm{TE}} + \overbrace{[\overline{V}]'\,[\overline{\mathrm{MSE}}]'}^{\mathrm{TOC}}}_{\mathrm{Transients}} dp, \qquad (3)$$

where $V$ is the meridional velocity and the vertical integral is over pressure ($p$) from the TOA to the surface; square brackets [ ] denote zonal averages, overbars $\overline{(\quad)}$ denote time averages

over each month of analysis, asterisks ($^*$) are departures from the zonal average, and primes ($'$) are departures from the time average. The calculation is performed at each latitude ($\theta$). The first term is the product of the time and zonal mean meridional velocity and MSE and represents the meridional overturning circulation energy transport (MOC) by way of the vertical gradient in MSE. We account for conservation of mass in the MOC energy transport by removing the vertically-averaged MSE (Marshall et al. 2013) as opposed to using a barotropic wind correction (Trenberth and Stepaniak 2003a) because the resultant MOC has been shown to be more physically relevant on monthly time scales (Liang et al. 2018). The second term is the stationary eddy energy transport (SE) which is poleward when the time average eddy (i.e. monthly mean, anomaly from zonal mean) poleward velocity occurs in a warm (or wet) sector. The first two terms can be calculated from monthly mean data.

The third term is the transient eddy energy transport (TE) due to the temporal covariance of $V$ and MSE that is primarily associated with baroclinic synoptic eddies. The fourth term is the energy transport associated with the covariance of the zonal mean overturning circulation and the vertical stratification that has previously been referred to as the transient overturning circulation (TOC; Marshall et al. 2013); it is two orders of magnitude smaller than the MOC in the deep tropics and two orders of magnitudes smaller than the eddy terms in the mid-latitudes. Thus, herein we will ignore the TOC in our discussion of AHT and refer to the sum of the TOC and transient eddy energy transport simply as TE although we note that the term "transients" would be a more technically accurate word choice. The moist and dry components of AHT, SE, MOC and TE are calculated from Eq. 3 by replacing the total MSE with the moist ($Lq$) and dry ($C_pT + gZ$) components, respectively.

OHT is calculated as the residual of the MHT determined from TOA radiation via Eq. 2 and the AHT calculated from the atmospheric reanalysis via Eq. 3 as in Trenberth and Caron (2001).

Stated otherwise, the satellite-derived TOA radiation and reanalysis-derived AHT convergence constrains the surface energy fluxes (as a residual) at each latitude via the atmospheric energy balance. The oceanic energy balance requires that the surface heat fluxes are balanced by the ocean heat transport divergence and, thus, the implied OHT($\theta$) is the spatial integral from the pole to $\theta$.

*b. Partitioning of MHT and AHT using monthly average coupled climate model output*

We partition AHT in the CMIP5 models using monthly mean data because the six-hourly output needed to calculate the transient eddy energy transport in Eq. 3 is not readily available for all models. However, the implied OHT at each latitude can be calculated accurately from the surface heat flux (SHF), which is composed from standard model output. The OHT is the spatial integral of the SHF over the polar cap bounded by that latitude:

$$\mathrm{OHT}(\theta) = -2\pi a^2 \int_{\theta}^{90} \cos(\Theta)\,[\mathrm{SHF}(\Theta)]\,d\Theta, \tag{4}$$

a statement that (in equilibrium) the surface heat flux out of the ocean, beyond a latitude circle, is balanced by poleward ocean energy transport into the region. SHF is the net (radiative plus turbulent) *downward* energy flux at the surface:

$$\mathrm{SHF} = \underbrace{\mathrm{SW}\downarrow - \mathrm{SW}\uparrow + \mathrm{LW}\downarrow - \mathrm{LW}\uparrow}_{\text{Surface Radiation}} - \underbrace{\mathrm{Sensible}\uparrow - \mathrm{Latent}\uparrow}_{\text{Turbulent}}, \tag{5}$$

where SW and LW refer to the shortwave and longwave radiative fluxes with arrows denoting downwelling and upwelling radiation at the surface. We note that Eq. 4 is valid when the ocean is in *equilibrium*. When the system is not in equilibrium (i.e. the ocean is accumulating energy), Eq. 4 expresses the *implied* OHT which is the sum of OHT and the spatial integral of the tendency in ocean heat content. Thus, our comparison of OHT diagnosed from Eq. 4 in the PI and LGM (equi-

librium) simulations versus the $4\times CO_2$ (transient) simulations do *not* constrain changes in OHT since the latter includes the impact of transient ocean storage. However, the change in AHT that accompanies changes in implied OHT is independent of whether the implied OHT change results from lateral ocean energy transport or transient ocean heat content changes since the atmosphere only responds to the associated SHF.

Total MHT is calculated as in the observations from the net TOA radiation via Eq. 2. AHT is then constrained by Eq. 1 as the residual of MHT and OHT calculated from TOA radiation and SHFs, respectively. Stated otherwise, the difference between TOA radiation and the (downward) SHF constrains the net (radiative plus diabatic) heating of a column of atmosphere which can be spatially integrated to calculate AHT. As in the observations, the AHT by the SE and MOC is calculated from the the monthly mean fields of $V$ and MSE via Eq. 3. The energy transport by transients (TE + TOC) is calculated as the residual of the atmospheric energy transport by the stationary circulation (SE + MOC) and the total AHT. As noted in our discussion of the observed AHT partitioning, TOC is much smaller than TE and we herein refer to the energy transport by the transients (calculated as a residual in the models) as TE for simplicity even though the TOC is also included in the calculation.

We next describe how to calculate the moist and dry components of AHT from monthly mean model output. The latent heat transport at any given latitude ($\mathrm{AHT}_{moist}(\theta)$) equals the integral of evaporation, $E$ minus precipitation, $P$, polewards of that latitude, multiplied by the latent heat of vaporization ($L$):

$$\mathrm{AHT}_{moist}(\theta) = -2\pi a^2 \int_{\theta}^{90} \cos(\Theta)\,[L(\mathrm{E}(\Theta) - \mathrm{P}(\Theta))]\,d\Theta. \tag{6}$$

The dry contribution to total AHT can then be calculated from the residual of total AHT and $\mathrm{AHT}_{moist}$. The moist and dry transport in the SE and MOC is calculated in the same manner as

the observations, by replacing MSE in Eq. 3 with the moist ($Lq$) and dry ($c_pT + gZ$) components. $\mathrm{TE}_{moist}$ is calculated as the residual of the total $\mathrm{AHT}_{moist}$ in Eq. 6 minus the sum of the latent heat transport by the steady atmospheric circulations ($\mathrm{SE}_{moist}$ and $\mathrm{MOC}_{moist}$):

$$\mathrm{TE}_{moist} = \mathrm{AHT}_{moist} - (\mathrm{SE}_{moist} + \mathrm{MOC}_{moist}). \tag{7}$$

$\mathrm{TE}_{dry}$ is the difference between the total TE and $\mathrm{TE}_{moist}$.

The above discussion pertains to the calculation of annual-mean AHT and OHT where (in an equilibrium climate) ocean and atmospheric energy content changes are negligible. On seasonal time scales, we must account for the tendency in atmospheric energy content in our calculation of AHT and seasonal storage of energy in the ocean in the interpretation of implied OHT. The implementation of these considerations is discussed in detail in the Appendix.

*c. Validation of partitioning technique*

The AHT partitioning method used on climate models uses monthly averaged model output and relies on the closure of the atmospheric energy budget to diagnose the transient eddy energy transport as the residual of that demanded by TOA radiation and surface fluxes minus the energy transport by the stationary circulation. Here, we analyze the closure of the atmospheric energy budget in a single climate model using high-frequency atmospheric fields alongside climatological energy fluxes at the TOA and surface as a validation of the accuracy of the methods based on monthly mean fields proposed above..

We run a 10 year PI simulation in the NCAR CESM coupled model and output the time averaged product of instantaneous (i.e. at each dynamic time step) V and T ($\overline{VT}$), V and Q ($\overline{VQ}$), and V and Z ($\overline{VZ}$) as a three dimensional field (pressure level, lat,lon). The output is interpolated to pressure levels from the model's native vertical coordinate akin to the CMIP archived data. This

choice was made to test if the interpolation to pressure levels introduces energy budget residuals. The transient MSE transport ($\mathrm{TE}_{direct}$) is calculated as the difference between the time averaged products minus the product of the time average fields:

$$\mathrm{TE}_{direct} = \frac{2\pi a \cos(\theta)}{g} \int_0^{P_s} c_p \left(\overline{VT} - \overline{V}\,\overline{T}\right) + L\left(\overline{VQ} - \overline{V}\,\overline{Q}\right) + g\left(\overline{VZ} - \overline{V}\,\overline{Z}\right) dp. \tag{8}$$

There is excellent agreement between TE energy transport calculated from the residual of total AHT and the stationary energy transport (solid red line in top panel Fig. 3) and the direct calculation of TE energy transport from the high frequency fields via Eq. 8 (dashed red line). Similarly, $\mathrm{TE}_{moist}$ calculated from the monthly mean fields via Eq. 7 (solid red line in bottom panel Fig. 3) is in excellent agreement with that calculated by Eq. 8 (dashed red line). These statements are equivalent to the statement that the energy and moisture budgets of the atmosphere in CESM are both closed. These results suggest that the residual method used in this manuscript accurately diagnoses the TE energy and moisture transport.

*d. Climate model experiments analyzed*

We analyze MHT partitioning in three different experiments performed as part of the CMIP5 suite of experiments: (i) Pre-industrial (PI) control simulations run to equilibrium; (ii) Abrupt carbon dioxide quadrupling ($4\times CO_2$) from the PI base state; and (iii) LGM simulations forced by reduced greenhouse gas concentrations, prescribed ice sheet topography and orbital parameters from 21,000 years ago (Braconnot et al. 2007a). We analyze all model simulations that are publicly available and that report all (monthly mean) output fields required for our analysis: precipitation, TOA radiation, radiative and turbulent energy fluxes at the surface and three dimensional atmospheric winds, temperature, geopotential height and specific humidity. In total, output from 20 different models are included in the PI and $4\times CO_2$ analyses and seven different models are in-

cluded in the LGM analyses. PI and LGM climatologies are calculated from the last 50 years of the simulations; climatologies for the $4\times CO_2$ simulations are calculated using years 50-100 after quadrupling.

## 3. Near-invariance of total meridional heat transport from the LGM to $4\times CO_2$

We now provide an overview of the MHT changes over the ensemble of climate simulations spanning the Last Glacial Maximum (LGM) to $4\times CO_2$ as viewed from the dynamics and radiative perspectives. We consider transport changes to be robust when the ensemble mean change exceeds two standard deviations of the mean change[1]. This criteria roughly corresponds to a 95% confidence interval of ensemble mean changes in a two tailed t-test.

In the ensemble average, total MHT in the LGM and $4\times CO_2$ simulations is nearly identical to that in the PI simulations: the CMIP5 ensemble average change in MHT is not significantly different from zero at all latitudes in the $4\times CO_2$ simulations and outside of the NH mid-latitudes in the LGM (Fig. 1b). However, while the total ensemble mean MHT is climate-state invariant (excluding the LGM changes in the NH) the component contributions to MHT vary substantially and robustly across simulations. Compensating changes are seen in the broadest sense– from a dynamics perspective (in the partitioning of MHT between AHT and OHT) and from a radiative perspective (in the changes in the equator-to-pole gradient of OLR and ASR). The changes in $\text{MHT}_{MAX}$ in each model under $4\times CO_2$ and LGM forcing are shown in Tables 1 and 2 respectively. $\text{MHT}_{MAX}$ changes within a single model can depart from the ensemble mean change by as much as 0.3 PW in both hemispheres due to inter-model differences in the (spatial structure of) cloud radiative feedbacks (see Fig. 6d of Zelinka and Hartmann 2012).

[1]The standard deviation of the mean change is the standard deviation of the change across models divided by the square root of the number of models.

From a dynamics perspective there is a robust increase in poleward atmospheric heat transport (AHT) under $4\times CO_2$ (Fig. 2b) in both hemispheres (Hwang and Frierson 2010) with nearly compensating decreases in implied poleward ocean heat transport (OHT, see Fig. 11B in Held and Soden 2006). The changes in implied OHT are due to the spatial pattern of transient ocean heat uptake that preferentially occurs in the high latitude oceans (Marshall et al. 2015; Armour et al. 2016). It is unclear whether the increase in poleward AHT and decrease in implied OHT under $4\times CO_2$ would also be a feature of the fully equilibrated $4\times CO_2$ climate (Chengfei et al. 2019). We can visualize the degree of compensation between AHT and OHT changes by co-plotting the magnitude of AHT and OHT at the latitude of maximum MHT (Fig. 2c) in both the NH (squares) and SH (circles); in this space, lines of constant $\mathrm{MHT}_{MAX}$ have slope of -1 and are shown by the colored contour lines. Changes in AHT and OHT (denoted by dashed lines and arrows) under $4\times CO_2$ (red) relative to the PI are primarily along lines of constant $\mathrm{MHT}_{MAX}$ in both the ensemble average and in individual models indicating near perfect compensation between AHT and OHT. AHT and OHT changes in the LGM simulations (blue lines and arrows in Fig. 2c) also compensate for each other but the compensation is not perfect as indicated by the drift of the blue lines across lines of constant $\mathrm{MHT}_{MAX}$. $\mathrm{MHT}_{MAX}$ increases robustly in the NH under LGM forcing and thus the ensemble-mean increase in poleward AHT in the NH is unaccompanied by compensating OHT changes.

From a radiative perspective, the MHT can only change if the equator-to-pole gradient of net radiation at the top of atmosphere (TOA) changes. In all three sets of simulations, the broad scale structure of absorbed solar radiation (ASR) and outgoing longwave radiation (OLR) are nearly unchanged (c.f. the red and blue lines in Fig. 1d) suggesting that the magnitude of MHT is constrained by Earth-Sun geometry to zeroth order in accordance with Stone (1978). Furthermore, changes in the equator-to-pole gradient of ASR and OLR nearly compensate for each other (Fig.

1d and 2e). For example, in response to $4\times CO_2$, extratropical ASR and OLR both increase (relative to their global mean values) as the high-latitude surface albedo decreases (Donohoe and Battisti 2011) and polar amplification (e.g Holland and Bitz 2003) enhances OLR via the Planck feedback leaving the net TOA radiative deficit over the extratropics nearly unchanged.

Donohoe and Battisti (2012) introduced a metric to formalize this radiative compensation over the polar cap bounded by the latitude ($\theta_{MAX}$) where MHT = $\text{MHT}_{MAX}$ in each hemisphere. Let $\text{ASR}^*$ be the the spatial integral of the deficit of ASR (relative to the global mean) poleward of $\theta_{MAX}$ and $\text{OLR}^*$ be the deficit of OLR over the same region, then $\text{MHT}_{MAX}$ = $\text{ASR}^*$- $\text{OLR}^*$. Fig. 2F shows that $\text{ASR}^*$ and $\text{OLR}^*$ each change by order 1PW in response to LGM and $4\times CO_2$ forcing with the most notable change being the robust increase of both quantities by more than 1PW in the NH in the LGM simulations (blue squares). However, the changes in $\text{ASR}^*$ and $\text{OLR}^*$ mostly compensate for one another (the changes denoted by the lines with arrows are almost parallel to the contour lines of constant $\text{MHT}_{MAX}$) and, thus, $\text{MHT}_{MAX}$ is nearly climate-state invariant despite large changes in the individual radiative components that constrain MHT. The only significant (ensemble mean) change in $\text{MHT}_{MAX}$ occurs in the NH under LGM conditions where the increase in $\text{ASR}^*$ exceeds that in $\text{OLR}^*$ (the solid blue line connecting squares has slope less than 1 in Fig. 1f). Interestingly, the net TOA radiation during the LGM changes substantially regionally with decreases of $\approx$60 W $\text{m}^{-2}$ over the Laurentide ice sheet (not shown) and zonal means decreases of $\approx$10 W $\text{m}^{-2}$ (c.f. the dashed and solid blue lines in Fig. 1d near 60°N) due to reduced ASR over the bright surface. However, there is a compensating increase in *net* TOA radiation poleward of 70°N due to decreased OLR associated with surface cooling that results in a near cancellation of $\text{OLR}^*$ and $\text{ASR}^*$. These results show that despite large regional scale net radiative changes, the equator-to-pole scale net TOA radiation, and thus $\text{MHT}_{MAX}$, is approximately invariant across vastly different climate states.

We have seen that $\mathrm{MHT}_{MAX}$ is nearly climate-state invariant because there is near compensation from both dynamical and radiative perspectives. From a dynamics perspective AHT and OHT changes nearly compensate. From a radiative perspective, $\mathrm{ASR}^*$ and $\mathrm{OLR}^*$ changes nearly compensate. We now look at a more detailed view of AHT changes partitioned into dynamic circulation changes and thermodynamic energy components.

## 4. Partitioning of heat transport: comparison of models and observations

We begin with a brief comparison between models and observations of the dynamic (TE, SE, MOC) and thermodynamic (moist, dry) AHT partitioning, in both the annual mean and the solstitial season DJF and JJA (Fig. 4). We note at the onset that the comparison between PI simulations and the observed climate system over the 2000-2016 time period is not an apples-to-apples comparison since the PI simulations represent a equilibrium climate state whereas the observed system is in transient adjustment to anthropogenic forcing. Comparison between PI and historic simulations find generally small (magnitudes less than 0.1 PW) differences in MHT and its partitioning between AHT and OHT. However, in all models the implied ocean heat transport (OHT) in the southern hemisphere is approximately 0.1 PW smaller over the 2000-2016 time period in the historic run as compared to that in pre-industrial simulation in the same model while AHT is larger by approximately the same amount. We speculate that this results from transient ocean heat uptake in the Southern Ocean in response to historic anthropogenic forcing and this would bias the observed OHT low relative to the PI simulations should the same process be occuring in nature. The annual mean AHT at the latitude of maximum poleward transport ($\mathrm{AHT}_{MAX}$) in CMIP5 PI control simulations generally exceeds the observationally based estimates; $\mathrm{AHT}_{MAX}$ exceeds the ERA reanalysis calculation in 19 (out of 20) models in the NH and in 17 models in the SH. Similarly, $\mathrm{AHT}_{MAX}$ exceeds the NCEP reanalysis calculation in 17 models in the NH and in all models in the

SH. This is primarily due to greater poleward TE during the winter season (red lines in Fig. 4b,c) and secondarily due to less equatorward energy transport in the Ferrel cell (mid-latitude MOC) in the models compared to the observational estimate (primarily in the winter). This is somewhat of a puzzle because the strength of the Ferrel cell is generally thought to be a direct consequence of TE energy transport (Peixoto and Oort 1992). Interestingly, the annual-mean SE energy transport in models is biased low relative to the observations throughout the NH, a result that is remarkably consistent between the different reanalysis products. This model bias stems from too weak transport of sensible energy during the boreal winter (c.f. the dashed and solid green lines in Fig. 4b) and too weak moisture transport in the monsoonal systems during the boreal summer (Fig. 4c).

In the tropics, energy transport by the meridional overturning circulation (MOC) varies substantially between CMIP5 models and the ensemble average is biased low compared to the observations (Fig. 4a-c) in both the NH (by 17% and 29% of the ERA and NCEP values, respectively) and SH (by 27% and 14% of the ERA and NCEP values, respectively). This bias results from too little transport into the subtropics of the winter hemisphere at the latitude of maximum MOC (about 20°N in Boreal winter and 20°S in Austral winter; Fig. 4b,c). In the deep tropics (nearby the equator) the TE is in the same sense as the MOC but it is much stronger in the models than in the observations; TE is 40% of the MOC transport near the equator in the models. In contrast, transport by TE is negligible near the equator in both observational data sets (Donohoe et al. 2013b). This model-observational mismatch is entirely due to dry TE (c.f. the dashed and solid red lines in Fig. 4e,f).

Appendix Fig. A1 shows a comparison of annual mean MHT partitioned into AHT and implied OHT in models and observations where the observational estimates of OHT are calculated from the difference of the CERES derived MHT and the NCEP/ERA reanalysis derived AHT. Observational MHT is within the model spread of MHT in both hemispheres despite the large inter-model spread

in MHT. However, in general, models have stronger than observed poleward AHT and weaker than observed poleward OHT especially in the SH. Because our observed OHT is derived from the residual of MHT and AHT and has no direct observational constraint we are reluctant to speculate on the dynamical cause of this apparent model bias.

The reader may be concerned that the model-observation mismatches highlighted above result from the different methodologies used to partition AHT in models and observations. There are two possible sources of methodological differences: (1) any sub-6 hourly co-variances will not be accounted for in the observational TE potentially leading to a low bias and (2) any non-energy conserving process in the models (e.g. Lucarini and Ragone 2011) may lead to inconsistencies between the MHT diagnosed from energetic requirements versus those from dynamic processes biasing the TE transport calculated as a residual in unknown ways. However, we note that biases in MOC and SE are comparable in magnitude to those in TE and the former two contributions are calculated in exactly the same way in models and observations. This suggest that there are genuine, large differences in the partitioning of MHT between CMIP models and observations.

## 5. Energy transport partitioning changes under $4\times CO_2$

Here we focus on the dynamical and thermodynamic contributions that contribute to the increase in poleward AHT under $4\times CO_2$. In Figures 5 to 7 we present the PI and $4\times CO_2$ analyses for the annual mean, DJF, and JJA, respectively. Each figure shows the MOC, SE, and TE contributions to AHT, and each contribution is in turn split into its dry and moist components. The left-hand panels show the two climatologies, and the right-hand panels show the differences. Each of the twenty ensemble members is plotted, together with the ensemble mean. In what follows, we highlight several specific aspects of the analyses that we have found noteworthy. For those interested in

exploring specific questions, the heat transport partitioning for all model are available in the online repository: `https://atmos.uw.edu/~aaron/cmip_AHT_partition/`.

The annual-mean total poleward AHT increases in both hemispheres $4\times CO_2$ and the change in AHT is smooth function of latitude (Fig. 5b). However, the changes in the dynamical components of AHT have a rich meridional structure. Some of the component changes are robust across the ensemble members whereas others vary in sign and magnitude across the ensemble. Notably, for each model the component changes sum to a smooth increase in total poleward AHT (Fig. 5b,d).

The robust changes in AHT partitioning under $4\times CO_2$ are:

- *An increase in poleward heat transport by transient eddies (TE) in the SH storm track regions (30°S - 60°S).* This occurs during winter and summer (Fig. 6h and 7h). The ensemble-mean increases are due entirely to a robust increase in TE moisture transport. Changes in TE dry transport are ambiguous with nearly an equal number of models simulating increases and decreases. There is a robust compensating increase in the equatorward energy transport in the thermally indirect Ferrel cell as would be expected from the robust increase in low-level eddy heat flux convergence on the poleward flank of the storm track, forcing ascent. The meridional temperature gradient increases slightly in this region (not shown) during all seasons due to delayed Southern Ocean warming. As a result, the meridional moisture gradient increases owing to nearly constant relative humidity and the non-linearity in Clausius Clapeyron. We speculate this strengthened meridional moisture gradient causes the enhanced poleward TE moisture transport.

- *An increase in poleward moisture transport by stationary eddies in the subtropics of both hemispheres (10°S-40°S and 10°N-50°N) during summer (Fig. 6f and 7f).* In the climatology, stationary waves associated with monsoon systems (Hurley and Boos 2015) are responsible

for the maximum in moisture transport by stationary eddies that peaks near 25° latitude in the summer hemisphere. The increased moisture transport by stationary eddies in the $4\times CO_2$ ensemble represents an intensification of these climatological transports (Fig. 6f and 7f) that are likely due to an increase in ambient atmospheric moisture (Hori and Ueda 2006).

- *Large, nearly compensating changes in tropical moist and dry energy transport.* In the PI climatology, the meridional overturning circulation transports moisture ($\approx$ 4 PW of latent energy) into the summer hemisphere in the lower branch of the Hadley cell and dry energy ($\approx$ 6 PW of sensible + potential) out of the summer hemisphere in the upper branch of the Hadley cell with a net energy transport ($\approx$ 2 PW) away from the summer hemisphere. Under $4\times CO_2$, the moistening of the surface and upward extension of the Hadley circulation as the tropopause rises results in an enhancement of the dry and moist energy transport in the MOC (Fig. 5j, 6j and 7j) with small net changes (Held and Soden 2006; Yang and Dai 2015).

- *Increases in poleward stationary eddy heat transport (SE) in the Southern Ocean ($\approx 60°S$.* These changes are most prevalent during JJA and are entirely due to changes in sensible energy transport (Fig. 7e).

There are several changes in AHT that differ markedly among ensemble members. Most notably, the changes SE and TE in the NH mid-latitudes during DJF (Fig. 6f,h). At 45°N during DJF, the poleward SE increases by 0.2 $\pm$ 0.7 PW and the poleward TE increases by +0.4 $\pm$ 0.6 PW, where the stated $\pm$ values are $2\sigma$ across the 20 ensemble members. The inter-model spread in TE and SE changes are strongly (R=-0.71) negatively correlated, resulting in a total AHT change of 0.6 $\pm$ 0.3 PW. This result suggests that the change in total AHT is more tightly constrained (by TOA radiation and SHF constraints) than the response of the individual circulation components. This implies a mechanism of compensation between the SE and TE changes.

The total mid-latitude TE change is a tug of war between moist and dry components (Fig. 5h). The poleward latent energy transport increases in all models (mean = 0.4 PW) and the dry TE transport decreases (mean = -0.1PW) in the majority of models but with remarkable spread (0.6 PW). In the mid-latitudes in all seasons, inter-model differences in dry TE tend to reduce the inter-model spread of total AHT changes and make the resultant total AHT changes a smoother function of latitude.

TE contribute more to cross equatorial AHT during the solstice seasons under $4\times CO_2$ (Fig. 6a and 7a). As discussed in Section 4, TE near the equator is larger in CMIP5 PI than in observational estimates. Under $4\times CO_2$ the MOC still accomplishes the majority of AHT but the amplitude of the TE during the solstitial seasons is approximately 60% of MOC. In DJF, the changes in TE near the equator under $4\times CO_2$ are comparable in magnitude to the change in MOC (Fig. 6b). This result raises concerns with attributing ITCZ shifts to changes in cross equatorial AHT demanded by the hemispheric scale energetics which assume the tropical AHT changes are due to MOC changes (Schneider et al. 2014; Donohoe et al. 2013b).

## 6. Energy transport partitioning changes under Last Glacial Maximum conditions

CMIP5 models robustly and unanimously simulate an increases in MHT in the NH in their LGM simulations (Fig. 8b – ensemble mean = +0.3PW) primarily due to increases in AHT (mean = +0.2 PW). AHT increases in 5 of the 7 models and decreases in the 2 models that have substantial increases in poleward OHT (Fig. 2b). In contrast, changes in MHT and AHT in the SH are close to zero in the ensemble average (Fig. 8a,b). The most striking change during the LGM is the ($\approx$+0.7PW) enhancement of the NH SE around 55°N during DJF (Fig. 9f) that is seen in all models and in the ensemble mean; it is associated with the atmospheric stationary wave that is generated by the Laurentide ice sheet (e.g. Li and Battisti 2008) and transports sensible heat poleward (Fig.

9f) in the mid and upper troposphere (not shown). In DJF, the increase in SE is compensated by a ($\approx$-0.7PW) decrease in TE that is displaced slightly equatorward of the SE change (Fig. 9b). The TE decrease is due to decreases in the poleward transport of both dry and moist energy (Fig. 9h). While a decrease in moisture transport by transient eddies is expected in a colder climate, the simultaneous decrease in dry TE is counter-intuitive in a climate with an enhanced equator-to-pole temperature gradient, where one might expect stronger storm tracks based on baroclinic instability (Eady 1949). However, eddy kinetic energy has been shown to decrease in most LGM simulations because the stationary wave generated by the Laurentide ice sheet reduces the upper level seeding of storms in the Atlantic domain (Donohoe and Battisti 2009). In the net, the DJF AHT in the NH is nearly unchanged during the LGM due to the compensation between SE and TE changes.

Interestingly, the ensemble-mean increase in AHT in the NH mid-latitudes during the boreal *summer* is primarily a result of enhanced poleward TE centered around $40°N$ (ensemble average change = 0.7PW; Fig. 10f) combined with smaller magnitude increase in SE centered around $50°N$ (ensemble average change = 0.3PW; Fig. 10 h).

In the SH, the total AHT and its partitioning is relatively unchanged in the LGM simulations (Figs. 8 a,b). The only significant change is a decrease in poleward moist TE that compensates for the increase in poleward dry TE which is most prevalent in the austral winter (Fig. 10h). The total TE change is not significantly different from zero. Moist-dry compensation of energy transport changes is also seen in the MOC. In JJA in the cross equatorial moist MOC into the NH decreases under LGM conditions with a nearly compensating decrease in dry MOC into the SH (Fig. 10i,j). Interestingly, the moist and dry changes in MOC transport during DJF are not simply a scalar change in the climatological transports (with the same underlying latitudinal structure); there is southward shift of the distribution during the LGM that is most evident in DJF (Fig. 9i,j) due to a southward Hadley cell (and ITCZ) shift.

## 7. Summary and conclusions

Despite the large inter-model spread in climatological MHT in CMIP5 pre-industrial models, the ensemble mean MHT is in close agreement with the MHT observed in the NH (Donohoe and Battisti 2012) and biased low on average in the SH (Trenberth and Fasullo 2010) with the inter-model spread spanning the observational value. However, the partitioning of MHT in models is somewhat different from the partitioning in observations: (i) SH OHT is too weak in all climate models (Fig. A1); (ii) NH mid-latitude TE is larger in climate models than that observed; and (iii) SE is weaker in the models than in observations especially in boreal winter (Fig. 4). Additionally, in the deep tropics, TEs provide a modest contribution to AHT in climate models whereas AHT is almost entirely by the MOC in the observations. Remarkably, the inter-model spread in total MHT poleward of $50^{\circ}$ in both hemispheres is small compared with the enormous spread in the component contributions (SE and TE) suggesting that relative weighting of the different transport processes is less constrained than is their net impact on the net TOA radiation. Furthermore, the large inter-model spread in MHT is primarily accomplished by inter-model differences in the TE sensible energy transport.

Total poleward meridional heat transport (MHT) is nearly invariant in an ensemble of models spanning from the LGM to the PI to a world with $CO_2$ quadrupled above PI levels; for example, the mean absolute magnitude of MHT change is 0.3 (0.1) PW and 0.2 (0.1) PW in the NH and SH respectively in response to LGM ($4\times CO_2$) forcing. However, the partitioning of MHT between AHT and implied OHT and between the various atmospheric circulations (SE, TE and, MOC) and energetic (moist and dry) contributions changes substantially with climate forcing. Some of the changes in MHT partitioning are robust across the ensemble of climate models including: (i) TE latent heat transport increases in a warmer/moister world with nearly compensating decreases in

TE sensible heat transport, (ii) the Hadley cell exports more sensible energy from the tropics to the subtropics in a warmer climate and imports more moisture into the tropics in the lower branch of the Hadley circulation, (iii) subtropical stationary waves associated with summer monsoons transport more moisture in a warmer world due to enhanced ambient humidity, (iv) implied OHT decreases under $4\times CO_2$ (due to high latitude ocean heat uptake) with a nearly compensating increase in AHT in both hemispheres and (v) in response to LGM topography (e.g. the Laurentide ice sheet), NH stationary eddy sensible heat transport increases during the boreal winter. Other changes in the partitioning of MHT vary substantially between climate models including the net (moist plus dry) change in transient eddy energy transport with warming and the change in mid-latitude stationary eddy energy transport under $4\times CO_2$. Overall, the changes in MHT are small and spatially smooth but the partitioning of those changes between circulations is larger in magnitude, highly variable in space, and differs between climate models (e.g. Fig. 5b and 8b).

Stone (1978) and Farneti and Vallis (2013) both speculated the $\mathrm{MHT}_{MAX}$ is insensitive to changes in climate state because the atmosphere is efficient at transporting energy. The compensating changes between energy transports in the different dynamical components (AHT, OHT, SE, TE, MOC) and between latent and sensible heat seen here are consistent with the notion of efficient atmospheric energy transport (Liu et al. 2018b). However, in a system with efficient dynamics, radiative forcing at the equator-to-pole scale is primarily balanced by MHT changes (Yang et al. 2016, 2015b). The lack of MHT changes under LGM forcing – which is substantial at the equator-to-pole scale (Braconnot et al. 2007b) – seems at odds with the paradigm of efficient dynamics. Additionally, radiative feedbacks have substantial structure at the equator-to-pole scale (Feldl and Roe 2013; Armour et al. 2013) which would also be expected to result in changes in MHT in the limit of efficient dynamics since the homogenization of temperature results in spa-

tially variant radiative response. We offer a possible explanation to reconcile this apparent paradox below.

An emerging body of work has argued that, in response to external forcing, atmospheric motions move energy from regions that are inefficient at radiating energy to space to regions that are efficient at radiating energy to space (Roe et al. 2015; Feldl and Roe 2013; Frierson and Hwang 2012) by diffusing moist static energy (Armour et al. 2019) – the sum of latent and sensible energy in the atmosphere. In the MSE diffusion framework, temperature changes in the deep tropics have a larger (factor of three) impact on AHT than equal magnitude temperature changes in the high latitudes (Liu et al. 2016) because of the exponential nature in the water vapor dependence on temperature at fixed relative humidity. This framework provides two complimentary perspectives on the near invariance of MHT in a changing climate:

- The temperature response in regions of weaker (negative) radiative feedbacks will be greater than that in regions of stronger (negative) radiative feedbacks resulting in smaller regional differences in the net radiative response (e.g. the temperature response times the feedback) (Armour et al. 2019) resulting in small changes in the MHT.

- Although forcing yields temperature changes that are polar amplified (because radiative feedbacks are less negative in the high latitudes, Armour et al. 2013, 2019) changes in moisture are greater in the tropics than in the polar regions. As a result, the meridional profile of the change in MSE is relatively flat Frierson et al. (2006) and there is little change in MHT.

The MSE diffusion framework provides an explanation for why TOA net radiation changes in response to climate forcing are substantial at local scales yet are nearly immutable at the equator-to-pole scale. For example, in the LGM simulations there is a substantial ($\approx$ 10 W m$^{-2}$) zonal mean decrease in net radiation at the TOA over the Laurentide ice sheet (where the reduction in

ASR exceeds that in OLR locally) but a nearly equal-magnitude increase in net radiation poleward of 70°N where the decrease in OLR associated with cooling is unaccompanied by compensating ASR changes (Fig. 2e) over the perennial sea ice. Even in the presence of substantial regional-scale solar forcing, adjustments in the atmospheric circulation spatially smooth the temperature response resulting in temperature and OLR changes in regions outside of the localized forcing which oppose the energetic input by the forcing. As a result, the equator-to-pole gradient in ASR and OLR ($ASR^*$ and $OLR^*$) show large magnitude, but nearly compensating changes (i.e. the near unit slope of changes in Fig. 2f) that render the MHT nearly climate-state invariant. In more general terms, dynamics are incredibly efficient at counteracting forcing at small scales and do so by smoothing temperature outside the region of forcing. The resultant spatially averaged radiation changes are constrained by the regions of most efficient radiative damping (Pierrehumbert 1995). Thus, although dynamics may be more efficient than the *spatial average radiative damping* of the climate system, the large scale climate forcing is primarily balanced by radiative feedbacks in the region of most efficient radiative damping, leaving the MHT nearly unchanged.

From a dynamics perspective, the component circulations (OHT, AHT, SE, TE, MOC, moist, and dry) that comprise MHT vary remarkably between models and across the ensemble of simulations analyzed here. The near invariance of total MHT is accomplished by several different compensating component changes which we list and discuss below:

**Implied OHT versus AHT change**: In response to $4\times CO_2$ the reduction in implied OHT associated with high latitude ocean heat uptake is nearly compensated for by an increase in AHT. This near compensation is expected given that changes in OHT and ocean heat uptake modify the energy input to the atmospheric column in nearly the same way that the climatological solar insolation impacts the atmospheric column to drive MHT: the majority of

649 the ASR measured at the TOA is absorbed at the surface which heats the surface and, in turn,
650 heats the atmosphere via upward turbulent energy fluxes. In this sense, one would expect the
651 AHT to respond to changes in implied OHT the same way it responds to a spatially localized
652 radiative heating.

653 **Moist versus dry energy transport changes**: Compensating changes in moist and dry AHT
654 are seen in both the mid-latitude TEs and the tropical Hadley cells (MOC) as the atmosphere
655 warms and moistens (cools and drys). In both regions, the climatological moisture transport
656 is enhanced with warming. These changes are expected from unchanged atmospheric cir-
657 culations with increased moisture. The enhanced moisture content of the lower troposphere
658 and slight increase in gross moist stability of the tropical atmosphere with warming (Chou
659 and Chen 2010; Ma et al. 2012; Wu and Tan 2013) leads to compensating changes in MOC
660 tropical moisture import and dry static energy export in the surface and upper branches of
661 the Hadley cell respectively with little net change (Hill et al. 2015). In the mid-latitudes,
662 the opposing changes in TE moist and dry transports with warming result from an enhanced
663 mid-latitude meridional gradient of moisture (which results from the non-linear Clausius-
664 Clapeyron equation) and reduced meridional temperature gradient (Held and Soden 2006).

665 **Stationary versus transient eddy heat transport changes**: The ensemble mean response
666 to the Laurentide ice sheet in the LGM features an increase in SE and a decrease in TE in
667 the NH. Additionally, although the change in SE in response to $4\times CO_2$ differs markedly be-
668 tween models, for each model the change in TE opposes the change in SE. As a result, the
669 net change in AHT is both smaller in magnitude and spatially smoother than the component
670 changes. Donohoe and Battisti (2009) argue that the poleward deflection of the LGM jet over
671 the Laurentide ice sheet steers storms away from the Atlantic storm track, thereby reducing

the seeding of storms and the zonally averaged storminess. This result suggest that enhanced stationary wave amplitude can directly reduced the zonal mean transient eddy strength by steering storms away from the baroclinic zone that support storm growth (Kaspi and Schneider 2013).

**Transient eddy versus meridional overturning circulation heat transport changes**: In the mid-latitudes, changes in the MOC in the Ferrel cell oppose changes in TE. Similarly, in the tropics during the solstice seasons, models have stronger TE out of the summer hemisphere than observed but weaker MOC than observed. We note that this compensation between MOC and TE is expected on theoretical grounds by the following mechanism. Vertical motion in the atmosphere is thermodynamically constrained such that the adiabatic cooling/heating balances the TE divergence/convergence minus the radiative damping to space. Thus, stronger mid-latitude TE cause enhanced upwelling on the poleward flank of the storm track and, by mass continuity, an enhanced MOC in the Ferrel cell with equatorward AHT. Similarly, the mid-latitude TE implicitly impacts the strength of the Hadley cell in even the most basic axially symmetric theory (Held and Hou 1980) by way of the diabatic cooling induced by TE divergence in the subtropics. The compensation between MOC and TE helps explain why changes in MHT are small and meridionally smooth because the vertical motion in the overturning circulation responds to the residual of the radiative fluxes and TE divergence. This mechanism seems to play an important role in moderating the strength of MHT in idealized models where radiation is modeled as a Newtonian cooling (Held and Suarez 1994) but we suspect plays a smaller role in an atmosphere with realistic radiative processes.

TE changes are central to all the compensating changes seen in this work and we hypothesize that the adjustment of TE is paramount to maintaining the near invariance of MHT by the follow-

ing mechanism: TE responds to changes in the spatial gradients of atmospheric diabatic heating independent of what process gives rise to the heating anomaly. Therefore, a regional change in radiative forcing, implied OHT divergence or SE divergence will lead to gradients in atmospheric heating that are efficiently smoothed out by TE. Thus, models may differ in simulating the local radiative response to forcing, the mechanical response of SEs or ocean heat uptake but these inter-model differences will be compensated by changes in TE that will act to smooth out the net radiative response. In this sense, TE render the large scale MHT insensitive to the details of radiation and dynamics by homogenizing the net radiative changes at the equator-to-pole scale.

## 8. Data Availability Statement

All data used in this work are publicly available through the World Climate Research Proram (WCRP) Coupled Model Inter-comparison Project 5 (CMIP5), European Center for Medium-Range Weather Forecast, National Center for Environmental Prediction and the National Aeronautics and Space Administration Langley Research Center websites. Please see citations within the data and methods section of this manuscript for more information.

*Acknowledgments.* We thank Edward Blanchard-Wrigglesworth for running the CESM simulations with saved instantaneous eddy co-variances. We also thank Isacc Held, Geof Vallis and two anonymous reviewers for thoughtful suggestions that helped expand and clarify the manuscript. AD's work was partially funded by the National Science Foundation Paleo Perspective on Climate Change (P2C2) Grant number AGS-1702827 and the NSF Antarctic Program Grant Number PLR 1643436. KCA received support from National Science Foundation Award AGS-1752796. LCH received support from the National Science Foundation Graduate Research Fellowship Program GRFP-2018266662.

# APPENDIX

## A1. Methodology for partitioning MHT, AHT and OHT over the seasonal cycle

We describe the additional steps that are taken to calculate the climatological seasonal cycle of the various components of energy transport which involves taking into account the energy and moisture storage in the atmospheric column. For example, the AHT into a polar cap is balanced by the net radiative input at TOA, minus the downward surface energy flux (SHF) and the atmospheric column energy tendency ($\text{Storage}_{atmos}$):

$$\text{AHT}(\theta)_{seasonal} = -2\pi a^2 \int_{\theta}^{90} \cos(\Theta)\,(\text{ASR} - \text{OLR} - \text{SHF} - \text{Storage}_{atmos})\,d\Theta, \qquad \text{(A1)}$$

which is derived from the combination of Eqs. 1, 3 and 4 with the addition of $\text{Storage}_{atmos}$. The atmospheric energy storage is derived from the monthly mean, three-dimensional atmospheric temperature and humidity:

$$\text{Storage}_{atmos} = \frac{1}{g}\int_{0}^{P_s} \frac{d}{dt}\,(c_p T + Lq)\,dp. \qquad \text{(A2)}$$

Note that the geopotential term ($gZ$) does *not* appear in the integrand because an atmosphere in hydrostatic balance can only raise its center of gravity by thermal expansion and this contribution is accounted by use of the heat capacity at constant pressure (Trenberth 1997). The time derivative in the integrand is calculated from the centered finite difference of temporally-adjacent monthly data; the surface pressure ($P_s$) in the limit of the integral is set to annual-mean values to maintain consistency with the mass balance used in the calculation of the MOC (Liang et al. 2018).

In principle, energy conservation demands that the globally-averaged TOA radiation is equal to the sum of SHF and $\text{Storage}_{atmos}$ thus ensuring that $\text{AHT}(\theta)_{seasonal}$ in Eq. A1 is independent of whether the integral is performed from $\theta$ to the North Pole or (the negative of that) from the South

pole to $\theta$. In practice, we remove the global mean of each term[2] prior to calculating the implied AHT to ensure zero transport through the poles. These global mean corrections are of order 1 W m$^{-2}$ for the net diabatic heating of the atmosphere which corresponding to an uncertainty in AHT$_{MAX}$ of 0.2 PW.

Similar adjustments for the atmospheric moisture tendency are made in the calculation of the poleward moisture transport from P-E:

$$\mathrm{AHT}(\theta)_{moist,\,seasonal} = -2\pi a^2 \int_{\theta}^{90} L\cos(\Theta)\left(\mathrm{E}(\Theta) - \mathrm{P}(\Theta) - \frac{1}{g}\int_0^{P_s}\frac{d}{dt}q(\Theta)dp\right)d\Theta. \qquad \text{(A3)}$$

Additional caution must be taken when interpreting the implied OHT from the surface heat fluxes via Eq. 4 on seasonal timescales because the surface heat flux is balanced by the sum of ocean heat transport divergence and ocean heat content changes, the latter of which has magnitudes of order 300 W m$^{-2}$ over the entire extratropics seasonally. On seasonal and inter-annual timescales, the surface energy budget in the extratropics is primarily a balance between SHF and the tendency in ocean heat content (Fasullo and Trenberth 2008b; Donohoe et al. 2013a). Hence, the implied OHT from Eq. 4 is more aptly termed the ocean heat transport plus storage. For this reason, we will only discuss OHT in the annual mean. The seasonal cycle in OHT can be calculated by subtracting the seasonally averaged surface heat flux from the tendency of the vertically integrated ocean heat content where the latter is calculated using the three dimensional ocean temperature output as in Donohoe et al. (2013a) and Armour et al. (2016). This endeavor is beyond the scope of the current work.

[2]The global mean TOA radiation and SHF are each of order 10 W m$^{-2}$ on seasonal timescales (Fasullo and Trenberth 2008a) due to the eccentricity of the Earth's orbit about the Sun, while the sum of global mean TOA radiation, SHF and Storage$_{atmos}$ is energetically constrained to be zero.

The seasonal SE and MOC atmospheric energy transport (and their moist/dry partitioning) are calculated using Eq. 3 with monthly-mean fields. The total AHT by the TE for each month is calculated as the residual of total AHT from Eq. A1 and the SE and MOC contributions. The moist TE transport is calculated from the residual of the total $\mathrm{AHT}_{moist,\,seasonal}$ using Eq. A3 and the moist SE and MOC transports. Lastly, the dry TE transport is calculated as the residual of the total TE AHT and the moist TE transport.

## References


Armour, K., C. Bitz, and G. Roe, 2013: Time-varying climate sensitivity from regional feedbacks. *J. Climate*, **26**, 4518–4534.

Armour, K., J. Marshall, J. Scott, A. Donohoe, and E. Newsom, 2016: Southern Ocean warming delayed by circumpolar upwelling and equatorward transport. *Nat. Geo. Sci.*, **9 (7)**, 549–554.

Armour, K., N. Siler, A. Donohoe, and G. Roe, 2019: Meridional atmospheric heat transport constrained by energetics and mediated by large-scale diffusion. *J. Climate*, **32 (12)**, 3655–3680, doi:10.1175/JCLI-D-18-0563.1.

Bjerknes, J., 1964: Atlantic air-sea interaction. *Adv. Geophys.*, **10**, 1–82.

Braconnot, P., and Coauthors, 2007a: Results of PMIP2 coupled simulations of the Mid-Holocene and Last Glacial Maximum - Part 1: Experiments and large-scale features. *Climates Past Discuss.*, 261–277.

Braconnot, P., and Coauthors, 2007b: Results of PMIP2 coupled simulations of the Mid-Holocene and Last Glacial Maximum - Part 2: Feedbacks with emphasis on the location of the ITCZ and mid- and high latitudes heat budget. *Climates Past Discuss.*, 279–296.

Chengfei, H., Z. Liuand, and A. Hu, 2019: The transient response of atmospheric and oceanic heat transports to anthropogenic warming. *Nature Climate Change*, **(222)**, doi:10.1038/s41558-018-0387-3.

Chou, C., and C. Chen, 2010: Depth of convection and the weakening of tropical circulation in global warming. *J. Climate*, **23**, 3019–3030.

Dee, D., and Coauthors, 2011: The ERA-Interim reanalysis: Configuration and performance of the data assimilation system. *Quart. J. Roy. Meteor. Soc.*, **137**, 553–597, URL https://www.ecmwf.int/en/forecasts/datasets/reanalysis-datasets/era-interim, [accessed 05-January-2018, https://www.ecmwf.int/en/forecasts/datasets/reanalysis-datasets/era-interim].

Donohoe, A., and D. Battisti, 2009: Causes of reduced north atlantic storm activity in a CAM3 simulation of the Last Glacial Maximum. *J. Climate*, **32**, 4793–4808.

Donohoe, A., and D. Battisti, 2011: Atmospheric and surface contributions to planetary albedo. *J. Climate*, **24 (16)**, 4401–4417.

Donohoe, A., and D. Battisti, 2012: What determines meridional heat transport in climate models? *J. Climate*, **25**, 3832–3850.

Donohoe, A., J. Marshall, D. Ferreira, K. Armour, and D. McGee, 2013a: The inter-annual variability of tropical precipitation and inter-hemispheric energy transport. *J. Climate*, **27 (9)**, 3377–3392.

Donohoe, A., J. Marshall, D. Ferreira, and D. McGee, 2013b: The relationship between ITCZ location and atmospheric heat transport across the Equator: From the seasonal cycle to the Last Glacial Maximum. *J. Climate*, **26 (11)**, 3597–3618.

Eady, E., 1949: Long waves and cyclone waves. *Tellus*, **1 (3)**, 33–52.

797 Enderton, D., and J. Marshall, 2009: Controls on the total dynamical heat transport of the atmo-
798 sphere and oceans. *J. Atmos. Sci.*, **66**, 1593–1611.

799 Farneti, R., and G. Vallis, 2013: Meridional energy transport in the coupled atmosphere ocean
800 system: Compensation and partitioning. *J. Climate*, **26**, 7151–7166.

801 Fasullo, J. T., and K. E. Trenberth, 2008a: The annual cycle of the energy budget: Part 1. Global
802 mean and land-ocean exchanges. *J. Climate*, **21**, 2297–2312.

803 Fasullo, J. T., and K. E. Trenberth, 2008b: The annual cycle of the energy budget: Part 2. Merid-
804 ional structures and poleward transports. *J. Climate*, **21**, 2313–2325.

805 Feldl, N., and G. Roe, 2013: The nonlinear and nonlocal nature of climate feedbacks. *J. Climate*,
806 **26**, 8289–8304.

807 Frierson, D., I. Held, and P. Z. Gotor, 2006: A gray-radiation aquaplanet moist GCM. Part i: Static
808 stability and eddy scale. *J. Climate*, **63**, 2548–2566.

809 Frierson, D. M. W., and Y.-T. Hwang, 2012: Extratropical influence on itcz shifts in slab ocean
810 simulations of global warming. *J. Climate*, **25**, 720–733.

811 Held, I., 2001: The partitioning of the poleward energy transport between the tropical ocean and
812 atmosphere. *J. Atmos. Sci.*, **58**, 943–948.

813 Held, I., and A. Hou, 1980: Nonlinear axially symmetric circulations in a nearly inviscid atmo-
814 sphere. *J. Atmos. Sci.*, **37**, 515–533.

815 Held, I., and B. Soden, 2006: Robust responses of the hydrological cycle to global warming. *J.*
816 *Adv. Model. Earth Sy.*, **19 (21)**, 5686–5699.

817 Held, I., and M. Suarez, 1994: A proposal for the intercomparison of the dynamical cores of
818 atmospheric general circulation models. *Bull. Amer. Meteor. Soc.*, **75 (10)**, 1825–1830.

819 Hill, S., Y. Ming, and I. Held, 2015: Mechanisms of forced tropical meridional energy flux change.
820 *J. Climate*, **28**, 1725–1742.

821 Hobbs, W., M. Palmer, and D. Monselesan, 2016: An energy conservation analysis of ocean drift
822 in the CMIP5 global coupled models. *J. Climate*, **29**, 1639–1653.

823 Holland, M. M., and C. Bitz, 2003: Polar amplification of climate in coupled models. *Climate*
824 *Dyn.*, **21**, 221–232.

825 Hori, M., and H. Ueda, 2006: Impact of global warming on the East Asian winter monsoon as
826 revealed by nine coupled atmosphere-ocean GCMs. *Geophys. Res. Lett.*, **33 (3)**, doi:10.1029/
827 2005GL024961.

828 Huang, Y., and M. Zhang, 2014: The implication of radiative forcing and feedback for meridional
829 energy transport. *Geophys. Res. Lett.*, **41**, 1665–1672, doi:10.1002/2013GL059079.

830 Hurley, J., and W. Boos, 2015: A global climatology of monsoon low-pressure systems. *Quart. J.*
831 *Roy. Meteor. Soc.*, **141 (680)**, 1049–1064.

832 Hwang, Y., and D. Frierson, 2010: Increasing atmospheric poleward energy transport with global
833 warming. *Geophys. Res. Lett.*, **37**, L24 807.

834 Hwang, Y., D. Frierson, and J. Kay, 2011: Coupling between arctic feedbacks and changes in
835 poleward energy transport. *Geophys. Res. Lett.*, **38**, L17 704, doi:10.1029/2011GL048546.

836 Johnson, G., J. Lyman, and N. Loeb, 2009: Improving estimates of Earth's energy imbalance. *Nat.*
837 *Clim. Chang.*, **6 (7)**, 639–640.

838 Kalnay, E., and Coauthors, 1996: The NCEP/NCAR 40-year reanal-
839 ysis project. *Bull. Amer. Meteor. Soc.*, URL https://www.esrl.noaa.
840 gov/psd/data/gridded/data.ncep.reanalysis.html, [accessed 07-January-2018,
841 https://www.esrl.noaa.gov/psd/data/gridded/data.ncep.reanalysis.html].

842 Kaspi, Y., and T. Schneider, 2013: The role of stationary eddies in shaping midlatitude storm
843 tracks. *J. Atmos. Sci.*, **70 (8)**, 2596–2613.

844 Li, C., and D. Battisti, 2008: Reduced atlantic storminess during last glacial maximum: evidence
845 from a coupled climate model. *J. Climate*, **21**, 3561–3579.

846 Liang, M., A. Czaja, R. Graversen, and R. Tailleux, 2018: Poleward energy transport: Is the
847 standard definition physically relevant at all time scales? *Climate Dyn.*, **50**, 1785–1797.

848 Liu, X., D. Battisti, and A. Donohoe, 2018a: Tropical precipitation and cross-equatorial ocean
849 heat transport during the mid-holocene. *J. Climate*, **30 (10)**, 3529–3547.

850 Liu, Z., C. He, and F. Lu, 2018b: Local and remote responses of atmospheric and oceanic heat
851 transports to climate forcing: Compensation versus collaboration. *J. Climate*, **31**, 6445–6460.

852 Liu, Z., H. Yang, C. He, and Y. Zhao, 2016: A theory for Bjerknes compensation: the role of
853 climate feedback. *J. Climate*, **29 (1)**, 1910 208.

854 Loeb, N. G., B. A. Wielicki, D. R. Doelling, G. L. Smith, D. F. Keyes, S. Kato, N. Manalo-Smith,
855 and T. Wong, 2009: Towards optimal closure of the Earth's top-of-atmosphere radiation budget.
856 *J. Climate*, **22**, 748–766.

857 Lorenz, E., 1953: A multiple index notation for describing atmospheric transport processes.
858 *AFCRL Report*, 35–53.

Lucarini, V., and F. Ragone, 2011: Energetics of IPCC4 AR4 climate models: energy balance and meridional enthalpy transports. *Rev. Geophys.*, **49**, RG1001.

Ma, J., S. Xie, and Y. Kosaka, 2012: Mechanisms for tropical tropospheric circulation change in response to global warming. *J. Climate*, **25**, 2979–2994.

Marshall, J., A. Donohoe, D. Ferreira, and D. McGee, 2013: The oceans role in setting the mean position of the Inter-Tropical Convergence Zone. *Climate Dyn.*, 14, doi:10.1007/s00382-013-1767-z.

Marshall, J., J. Scott, K. Armour, J. Campin, M. Kelley, and A. Romanou, 2015: The oceans role in the transient response of climate to abrupt greenhouse gas forcing. *Climate Dyn.*, **44 (7-8)**, 2287–2299.

Masuda, K., 1988: Meridional heat transport by the atmosphere and ocean: anlysis of FGGE data. *Tellus*, **40A**, 285–302.

Oort, A., 1971: The observed annual cycle in the meridional transport of atmospheric energy. *J. Atmos. Sci.*, **28**, 325–339.

Oort, A., and T. V. Haar, 1976: On the observed annual cycle in the ocean–atmosphere heat balance over the Northern Hemisphere. *J. Phys. Oceanogr.*, **6**, 781–800.

Peixoto, J., and A. Oort, 1992: *Physics of Climate*. AIP Press, 160 pp pp.

Pierrehumbert, R., 1995: Thermostats, radiator fins, and the local runaway greenhouse. *J. Atmos. Sci.*, **52**, 1784–1806.

Priestley, C., 1948: Heat transport and zonal stress between latitudes. *Quart. J. Roy. Meteor. Soc.*, **75**, doi:28-40.

Rencurrel, M., and B. Rose, 2020: The efficiency of the Hadley cell response to wide variations in ocean heat transport. *J. Climate*, **33**, 1643–1658.

Rencurrell, M., and B. Rose, 2018: Exploring the climatic response to wide variations in ocean heat transport on an aquaplanet. *J. Climate*, **31 (16)**, 6299–6318.

Roe, G., N. Feldl, K. Armour, Y.-T. Hwang, and D. Frierson, 2015: The remote impacts of climate feedbacks on regional climate predictability. *Nat. Geo. Sci.*, **8**, 135–139, doi:10.1038/ngeo2346.

Schneider, T., T. Bischoff, and G. Haug, 2014: Migrations and dynamics of the Intertropical Convergence Zone. *nature*, **513**, 45–53.

Stone, P., 1978: Constraints on dynamical transports of energy on a spherical planet. *Dynam. Atmos. Oceans*, **2**, 123–139.

Taylor, K., R. Stouffer, and G. Meehl, 2012: An overview of CMIP5 and the experiment design. *Bull. Amer. Meteor. Soc.*, **93**, 485–498.

Trenberth, K. E., 1997: Using atmospheric budgets as a constraint on surface fluxes. *J. Climate*, **10**, 2796–2809.

Trenberth, K. E., and J. M. Caron, 2001: Estimates of meridional atmosphere and ocean heat transports. *J. Climate*, **14**, 3433–3443.

Trenberth, K. E., and J. T. Fasullo, 2010: Simulation of present day and 21st century energy budgets of the southern oceans. *J. Climate*, **23**, 440–454.

Trenberth, K. E., and D. P. Stepaniak, 2003a: Co-variability of components of poleward atmospheric energy transports on seasonal and interannual timescales. *J. Climate*, **16**, 3691–3705.

Trenberth, K. E., and D. P. Stepaniak, 2003b: Seamless poleward atmospheric energy transports and implications for the Hadley circulation. *J. Climate*, **16**, 3706–3722.

Trenberth, K. E., and D. P. Stepaniak, 2004: The flow of energy through the Earth's climate system. *Quart. J. Roy. Meteor. Soc.*, **130**, 2677–2701.

Vallis, G., and R. Farneti, 2009: Meridional energy transport in the coupled atmosphere ocean system: Scaling and numerical experiments. *Quart. J. Roy. Meteor. Soc.*, **135**, 1643–1660.

Vellinga, M., and P. Wu, 2008: Relations between northward ocean and atmosphere energy transports in a coupled climate model. *J. Climate*, **21**, 561–575.

Vonder Haar, T., and A. Oort, 1973: New estimate of annual poleward energy transport by Northern Hemisphere oceans. *J. Phys. Oceanogr.*, **2**, 169–172.

Wielicki, B., B. Barkstrom, E. Harrison, R. Lee, G. Smith, and J. Cooper, 1996: Clouds and the Earth's radiant energy system (CERES): An Earth observing system experiment. *Bull. Amer. Meteor. Soc.*, **77**, 853–868.

Wu, T., and P. Tan, 2013: Changes in gross moist stability in the tropics under global warming. *Climate Dyn.*, **41**, 2481–2496.

Wu, Y., M. Ting, R. Seager, H. Huang, and M. Cane, 2011: Changes in storm tracks and energy transports in a warmer climate simulated by the GFDL CM2.1 model. *Climate Dyn.*, **37**, 53–72.

Xiang, Z., M. Zhao, Y. Ming, W. Yu, and S. Kang, 2018: Contrasting impacts of radiative forcing in the Southern Ocean versus southern tropics on ITCZ position and energy transport in one GFDL climate model. *J. Climate*, **31 (14)**, 5609–5628.

Yang, H., and H. Dai, 2015: Effect of wind forcing on the meridional heat transport in a coupled climate model: equilibrium response. *Climate Dyn.*, **45**, 1451–1470.

Yang, H., Q. Li, K. Wang, Y. Sun, and D. Sun, 2015a: Decomposing the meridional heat transport in the climate system. *Climate Dyn.*, **44 (9)**, 2751–2768.

Yang, H., Y. Zhao, Q. Li, and Z. Liu, 2015b: Heat transport in atmosphere and ocean over the past 22,000 years. *Nat. Sci. Rep.*, **5**, doi:10.1038/srep16661.

Yang, H., Y. Zhao, and Z. Liu, 2016: Understanding Bjerknes compensation in atmosphere and ocean heat transports using a coupled box model. *J. Climate*, **29 (6)**, 2145–2160.

Zelinka, M., and D. Hartmann, 2012: Climate feedbacks, and their implications for poleward energy flux changes in a warming climate. *J. Climate*, **25**, 608–624.

# LIST OF TABLES

TABLE 1: $MHT_{MAX}$ in each model's PI simulation and its change under $4\times CO_2$ forcing.

| | **Northern Hemisphere** | | **Southern Hemisphere** | |
|---|---|---|---|---|
| | PI $MHT_{MAX}$ | $\Delta$ $MHT_{MAX}$ | PI $MHT_{MAX}$ | $\Delta$ $MHT_{MAX}$ |
| ACESS1.0 | 5.28 | 0.00 | 4.75 | -0.10 |
| BCC CSM1 | 5.69 | +0.05 | 5.27 | +0.06 |
| CAN ESM2 | 5.46 | +0.13 | 5.55 | -0.14 |
| NCAR CCSM4 | 5.57 | -0.06 | 5.32 | +0.20 |
| CNRM CM5 | 5.41 | -0.03 | 5.01 | -0.12 |
| CSIRO MK5 | 5.16 | +0.33 | 4.71 | -0.29 |
| FGOALS S2 | 5.52 | -0.11 | 5.45 | +0.09 |
| GISS E2R | 5.21 | +0.11 | 4.89 | -0.05 |
| GFDL CM3 | 6.03 | -0.15 | 5.57 | -0.31 |
| GFDL ESMG | 5.86 | +0.11 | 4.89 | -0.26 |
| GFDL ESM2M | 5.77 | +0.15 | 4.91 | -0.21 |
| INMCM4 | 5.38 | -0.02 | 5.17 | -0.02 |
| IPSL CM5A | 5.42 | -0.08 | 6.04 | -0.14 |
| IPSL CM5B | 5.42 | +0.14 | 5.89 | +0.00 |
| MIROC5 | 4.90 | +0.10 | 4.72 | -0.16 |
| MIROC ESM | 5.41 | -0.15 | 5.59 | +0.24 |
| MPI ESM P | 5.97 | -0.13 | 5.77 | -0.30 |
| MPI ESM LR | 5.90 | +0.23 | 5.78 | +0.31 |
| MRI CGCM3 | 5.76 | 0.00 | 5.08 | +0.02 |
| NOR ESM1 | 5.63 | -0.15 | 5.31 | +0.09 |
| Ensemble mean | 5.54 | +0.03 | 5.26 | +0.07 |

TABLE 2: $MHT_{MAX}$ in each model's PI simulation and its change under LGM forcing.

| | **Northern Hemisphere** | | **Southern Hemisphere** | |
|---|---|---|---|---|
| | PI $MHT_{MAX}$ | $\Delta$ $MHT_{MAX}$ | PI $MHT_{MAX}$ | $\Delta$ $MHT_{MAX}$ |
| MRI CGCM3 | 5.76 | 0.00 | 5.08 | -0.14 |
| NCAR CCSM4 | 5.57 | +0.48 | 5.32 | -0.30 |
| CNRM CM5 | 5.41 | 0.00 | 5.01 | +0.06 |
| IPSL CM5 LR | 5.11 | +0.30 | 6.06 | +0.27 |
| MIROC ESM | 5.41 | +0.57 | 5.59 | +0.10 |
| MPI ESM P | 5.97 | +0.27 | 5.77 | +0.22 |
| GISS E2 R | 5.21 | +0.46 | 4.89 | +0.07 |
| Ensemble mean | 5.49 | +0.30 | 5.39 | +0.04 |

# LIST OF FIGURES

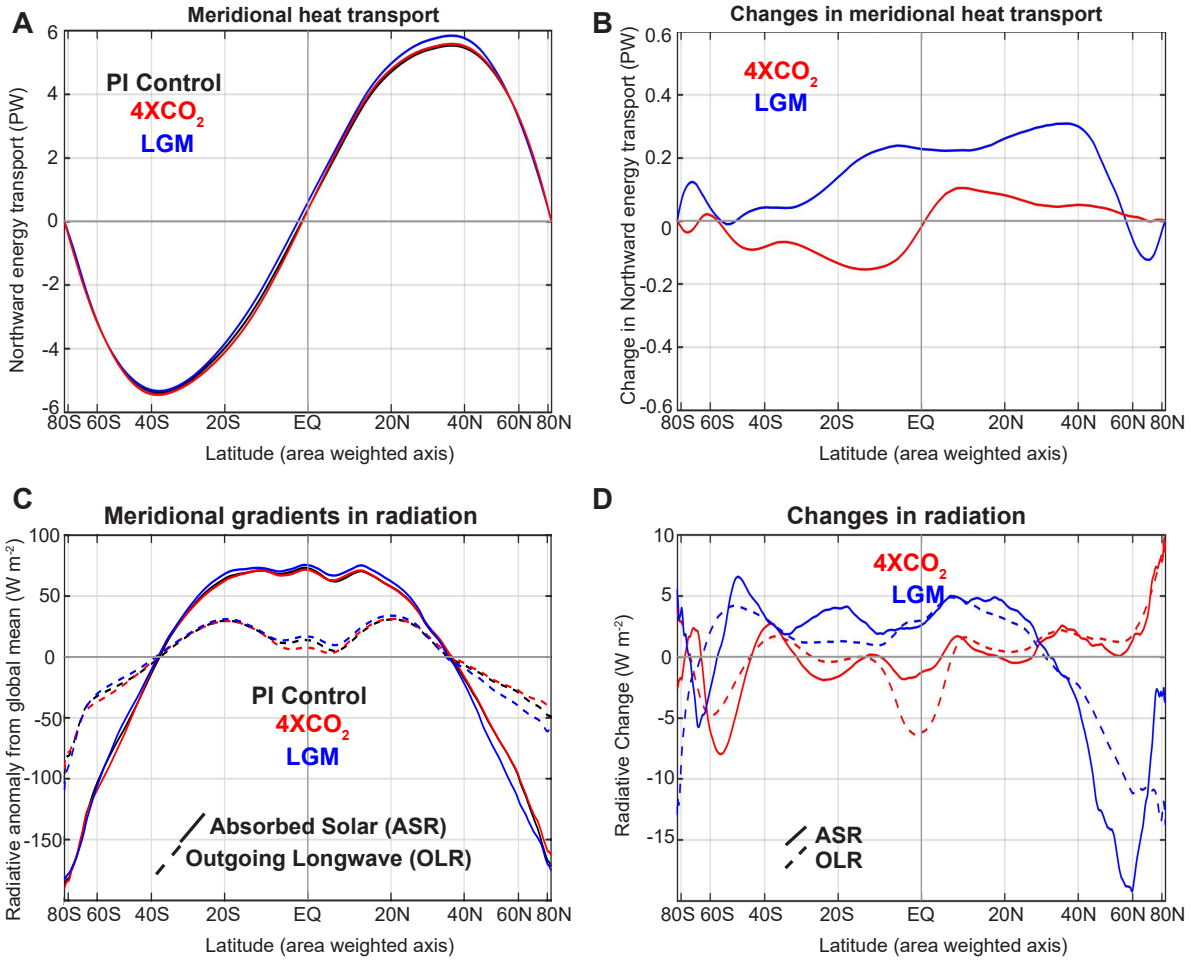


FIG. 1: (A) Ensemble averaged total (ocean plus atmosphere) annual mean meridional heat transport (MHT) in pre-industrial (PI; black), abrupt carbon dioxide quadrupling ($4\times CO_2$; red) and, last glacial maximum (LGM; blue) CMIP5 simulations. Only the seven models that span all three simulations are included in the ensemble average. (B) The changes in MHT between the $4\times CO_2$ and PI simulations (red), and between the LGM and PI simulations (blue). (C) Ensemble averaged annual- and zonal- mean radiation in PI (black), $4\times CO_2$ (red) and, LGM (blue). Solid lines show the net solar radiation at TOA (absorbed solar radiation; ASR) and dashed lines show the outgoing longwave radiation (OLR). The global mean has been removed from ASR and OLR to emphasize the meridional gradients. (D) The changes in ASR (solid) and OLR (dashed), with global mean removed, between the $4\times CO_2$ and PI simulations (red), and between the LGM and PI simulations (blue).

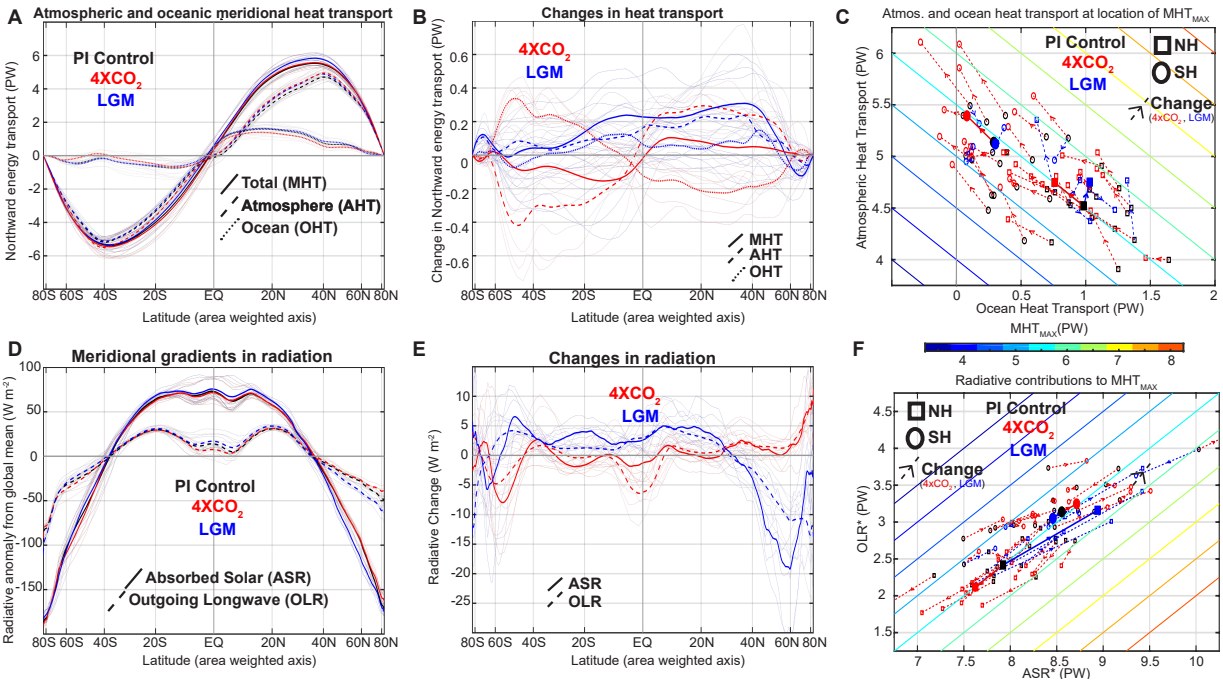


FIG. 2: (A) Annual-mean meridional heat transport (MHT; solid) partitioned between the atmosphere (AHT; dashed) and ocean (OHT; dotted) in pre-industrial (PI; black), abrupt carbon dioxide quadrupling ($4\times CO_2$; red) and, last glacial maximum (LGM –blue) CMIP5 simulations. Thin lines show individual models and thick lines show the ensemble-average. (B) The changes in MHT (solid), AHT (dashed) and, OHT (dotted) between the $4\times CO_2$ and PI simulations (red), and between the LGM and PI simulations (blue). (C) Scatter plot of OHT and AHT at the latitude where MHT achieves its maximum value ($MHT_{MAX}$) in each hemisphere. Squares show the Northern Hemisphere (NH) and circles show the Southern Hemisphere. Larger, filled markers represent the ensemble means. The dashed lines with arrows show the changes between the PI and $4\times CO_2$ (red), and between the PI and LGM (blue) simulations, respectively, using the same model. Colored contours show lines of constant $MHT_{MAX}$ with colors in the colorbar below. (D) Annual and zonal mean radiation in PI (black), $4\times CO_2$ (red) and, LGM (blue): ASR (solid) and OLR (dashed). The global mean has been removed from all fields to emphasize the meridional gradients. (E) Changes in ASR (solid) and OLR (dashed) between the $4\times CO_2$ and PI simulations (red), and between the LGM and PI simulations (blue). (F) Scatter plot of contribution of ASR gradients ($ASR^*$; abscissa) and OLR gradients ($OLR^*$; ordinate) to $MHT_{MAX}$. Symbols, lines and colorbar are as in panel C.

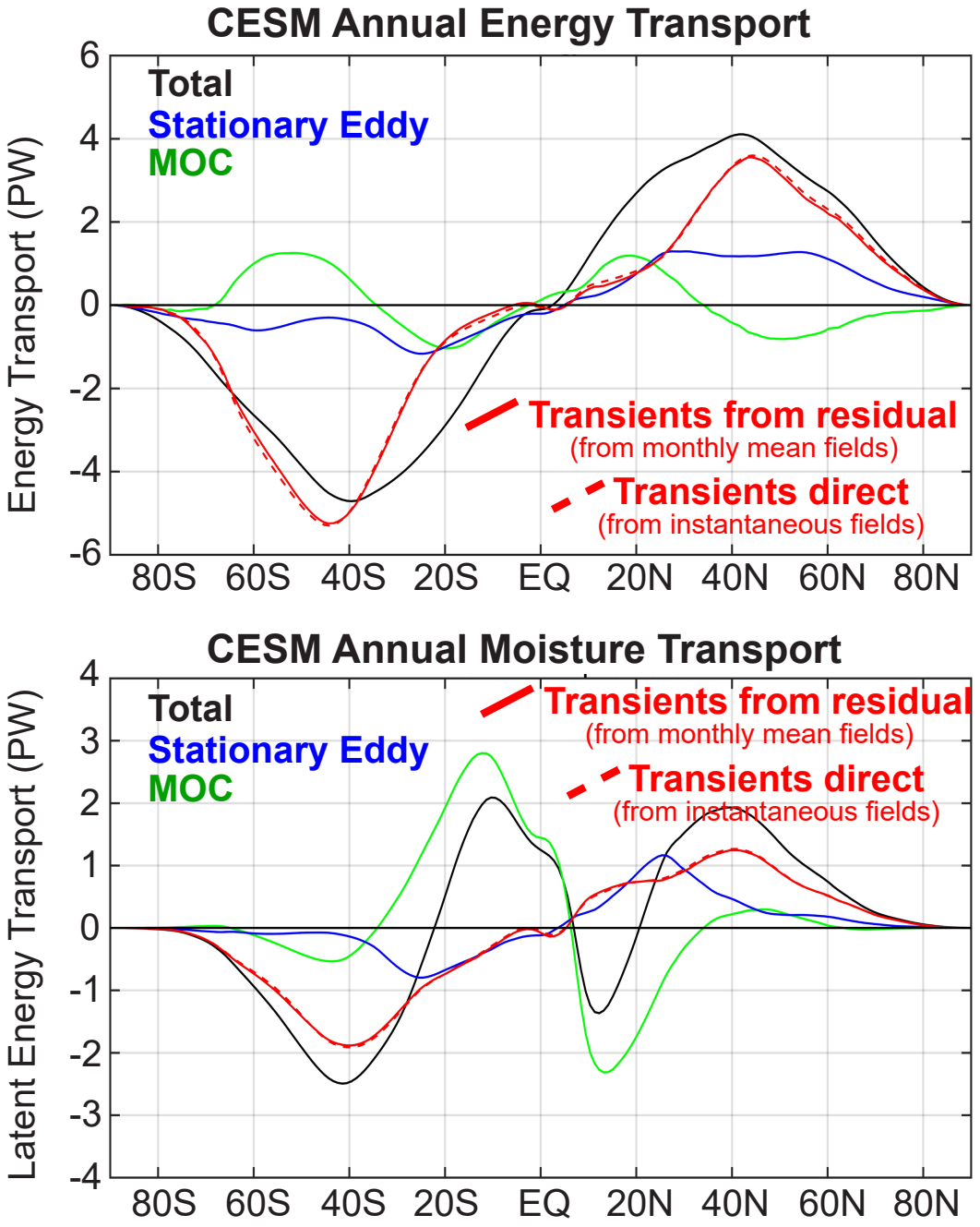


FIG. 3: (Top panel) Comparison of the zonally and vertically integrated transient eddy energy transport in CESM calculated using the **residual method** (section 2b – solid red lines) and the **direct method** (section 2a - dashed red lines). (Top panel) The total annual mean atmospheric energy transport. (Bottom panel) The annual mean atmospheric moisture transport.

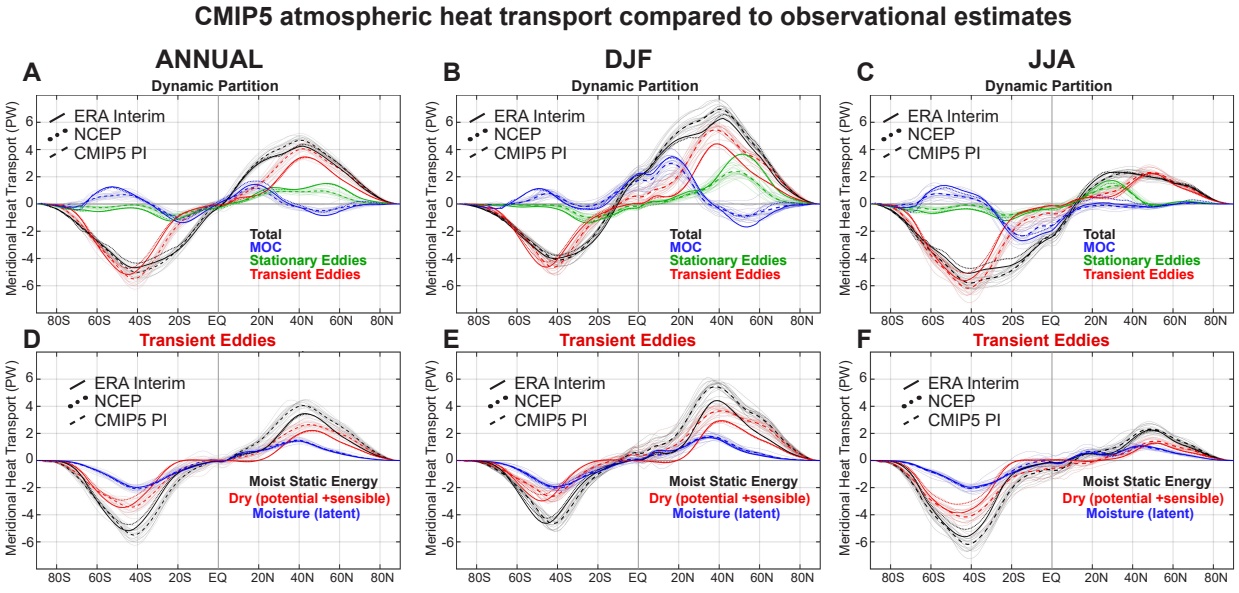


FIG. 4: (Top panels) Atmospheric meridional heat transport calculated from atmospheric reanalysis (solid line, ERA; dotted line, NCEP) and CMIP5 PI simulations (dashed) with thin line representing individual models and thick lines showing the ensemble-average. The total moist static energy transport is partitioned into component circulation contributions: meridional overturning circulation (MOC; blue), stationary eddies (green) and transient (red). (Bottom panels) The transient contribution to meridional energy transport broken down into moist (latent, blue) and dry (potential + sensible, red) contributions. The left panels show annual mean, the middle panels show DJF and and right panels show JJA)

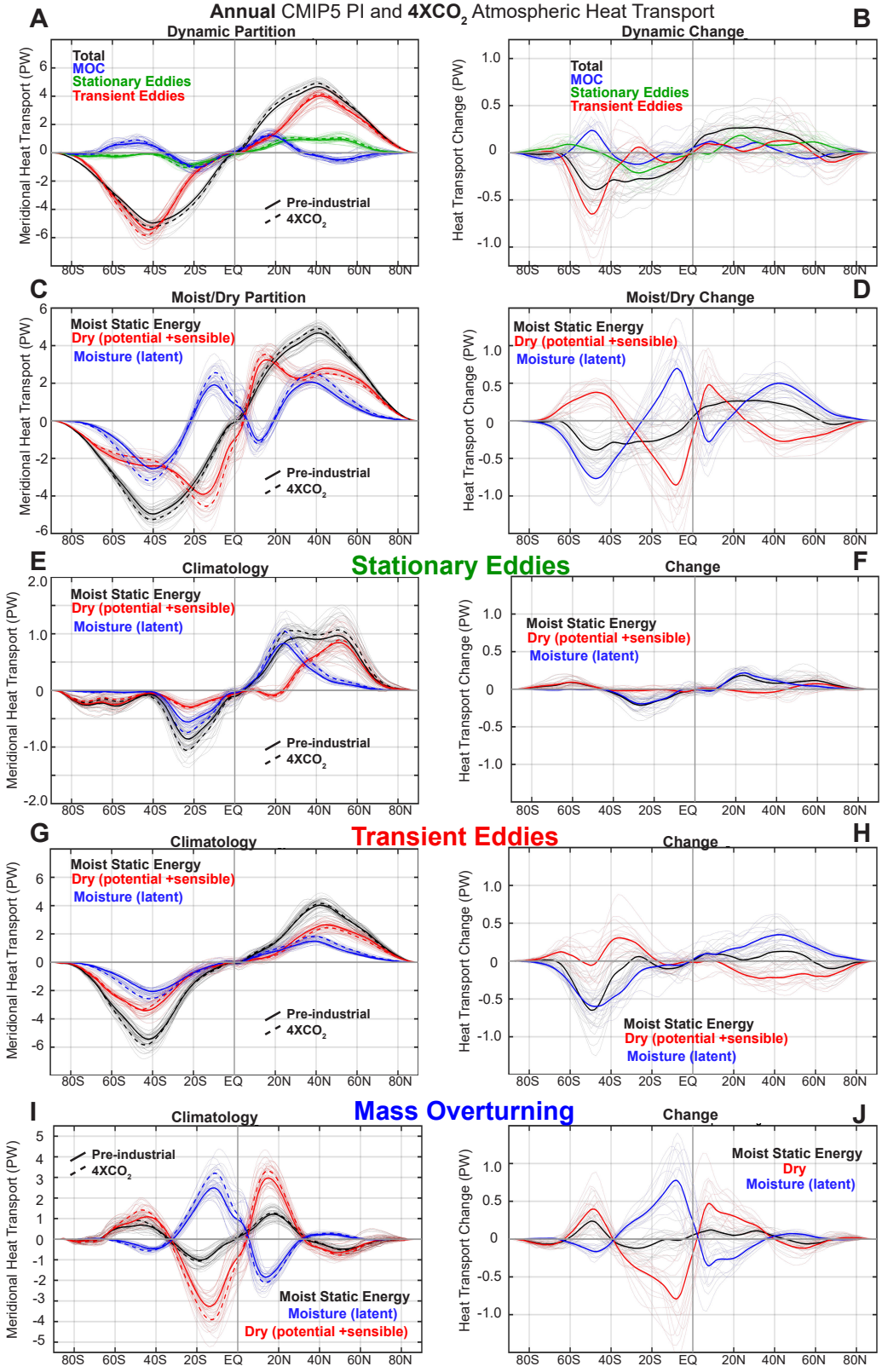


FIG. 5: (Left panels) Annual mean atmospheric energy transport in CMIP5 PI (solid lines) and $4\times CO_2$ (dashed lines) simulations and (right panels) the changes between $4\times CO_2$ and PI. (Top row) The partitioning of energy transport into atmospheric circulations type: MOC (blue), stationary eddies (green) and transient eddies (red) with total shown in black. (Second row) The partitioning of energy transport by energy type: dry (potential plus sensible, red) and moist (latent; blue). The bottom three rows show the moist and dry contributions within each circulation type: (third row) stationary eddies, (fourth row) transient eddies and (bottom row) MOC. Note that the range on the y-axis differs between the left hand panels and the all the right hand panels have the same range on the y-axis.

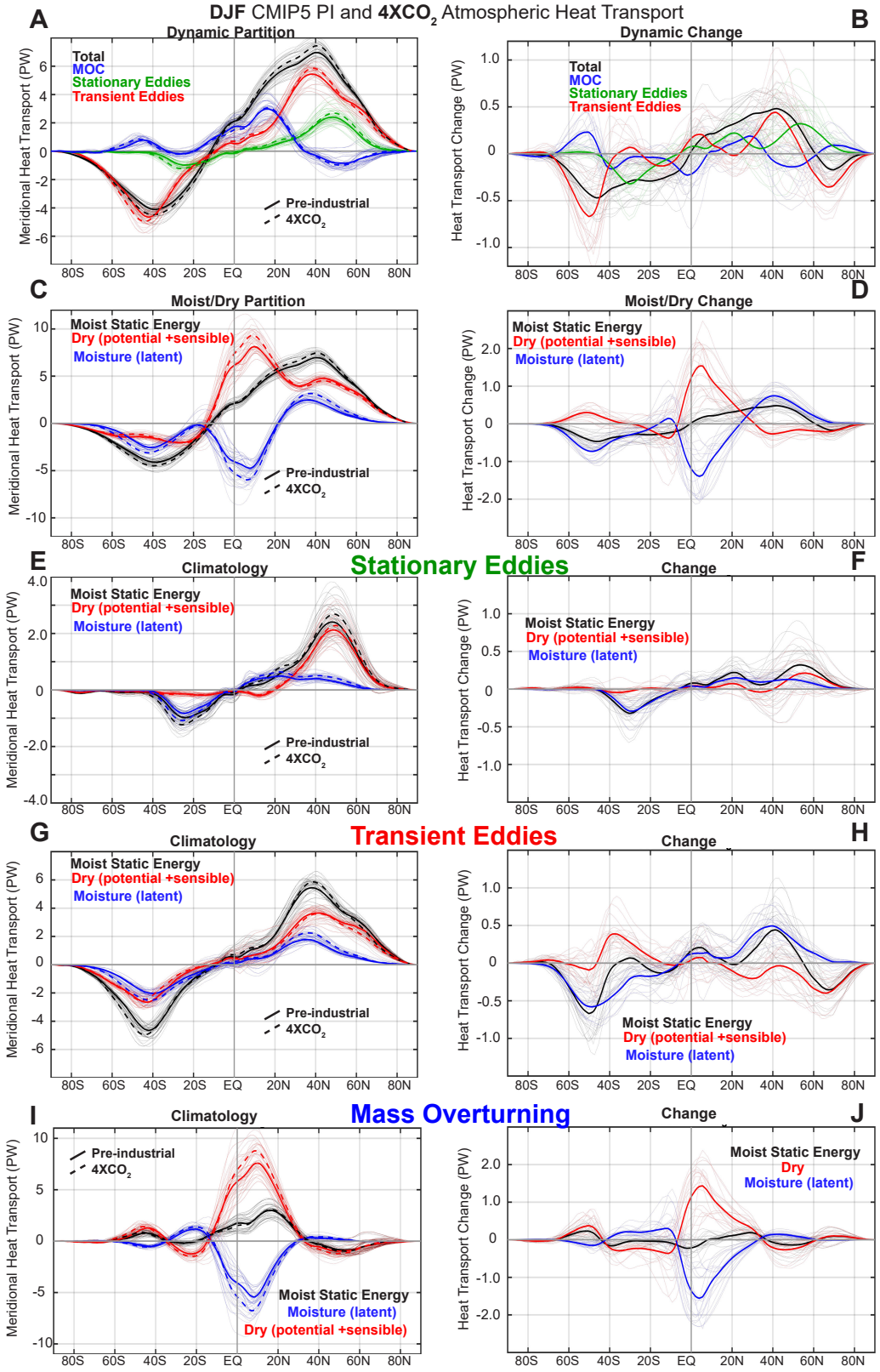


FIG. 6: As in Figure 5 except for December-January-February (DJF). Note that the range on the y-axis has been doubled relative to Figure 5 in the moist/dry partitioning (panels C and D), the MOC transport (panels I and J) and the climatological stationary eddy transport (panel E)

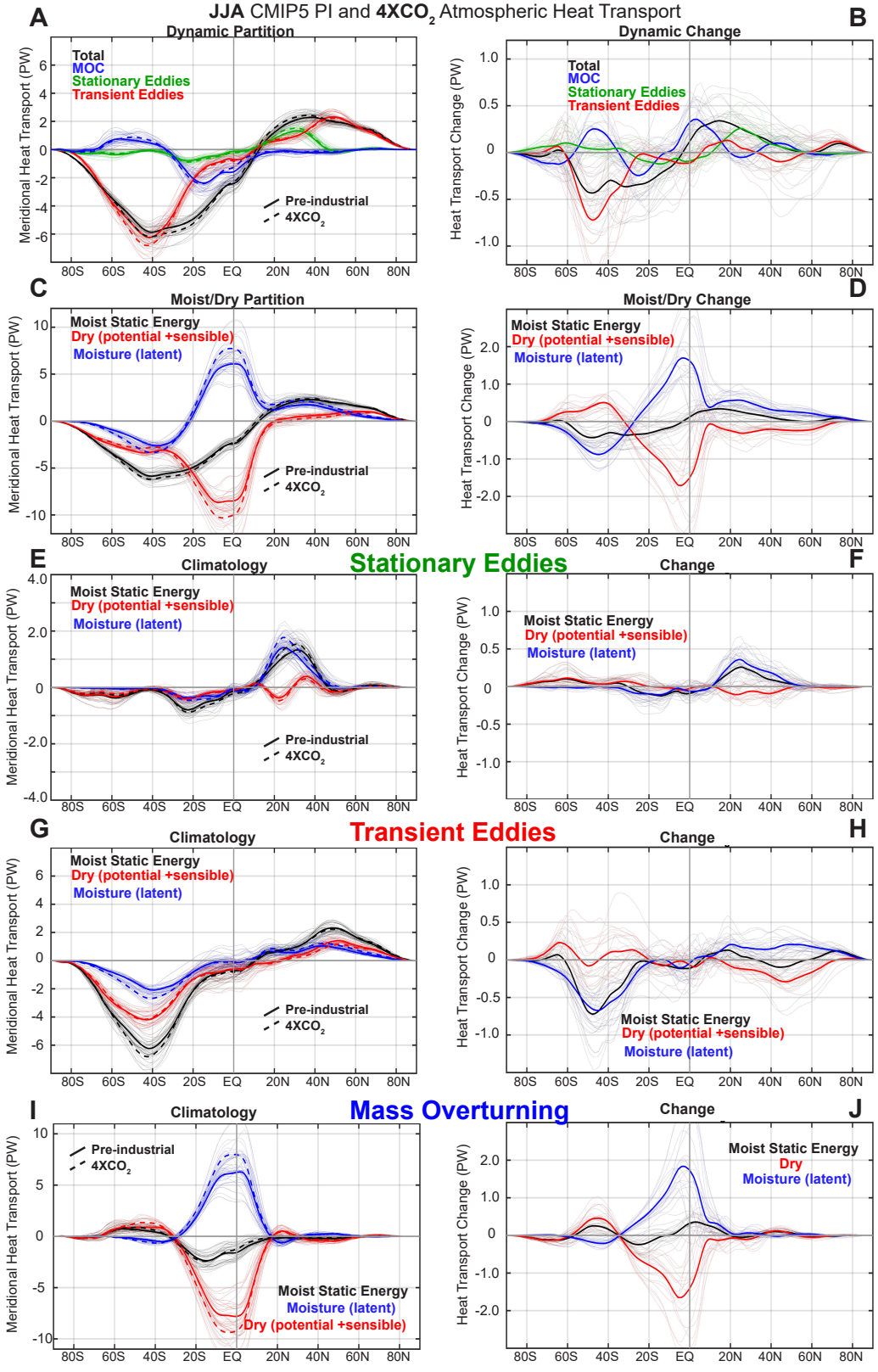


FIG. 7: As in Figure 5 except for June-July-August (JJA).

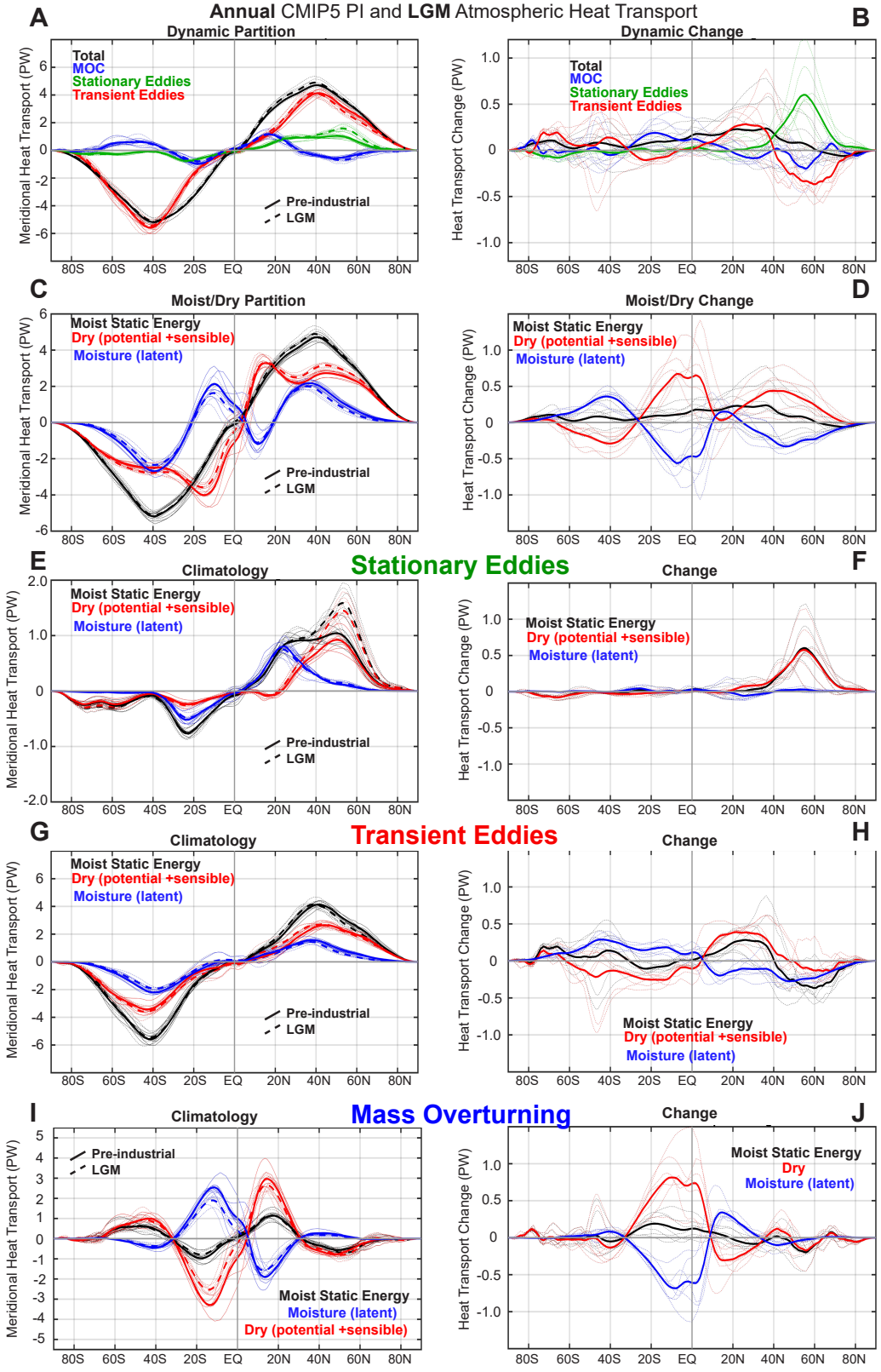


FIG. 8: As in Fig 5, except for PI (solid) and LGM (dashed) in the left columns and LGM-PI changes in the right columns.

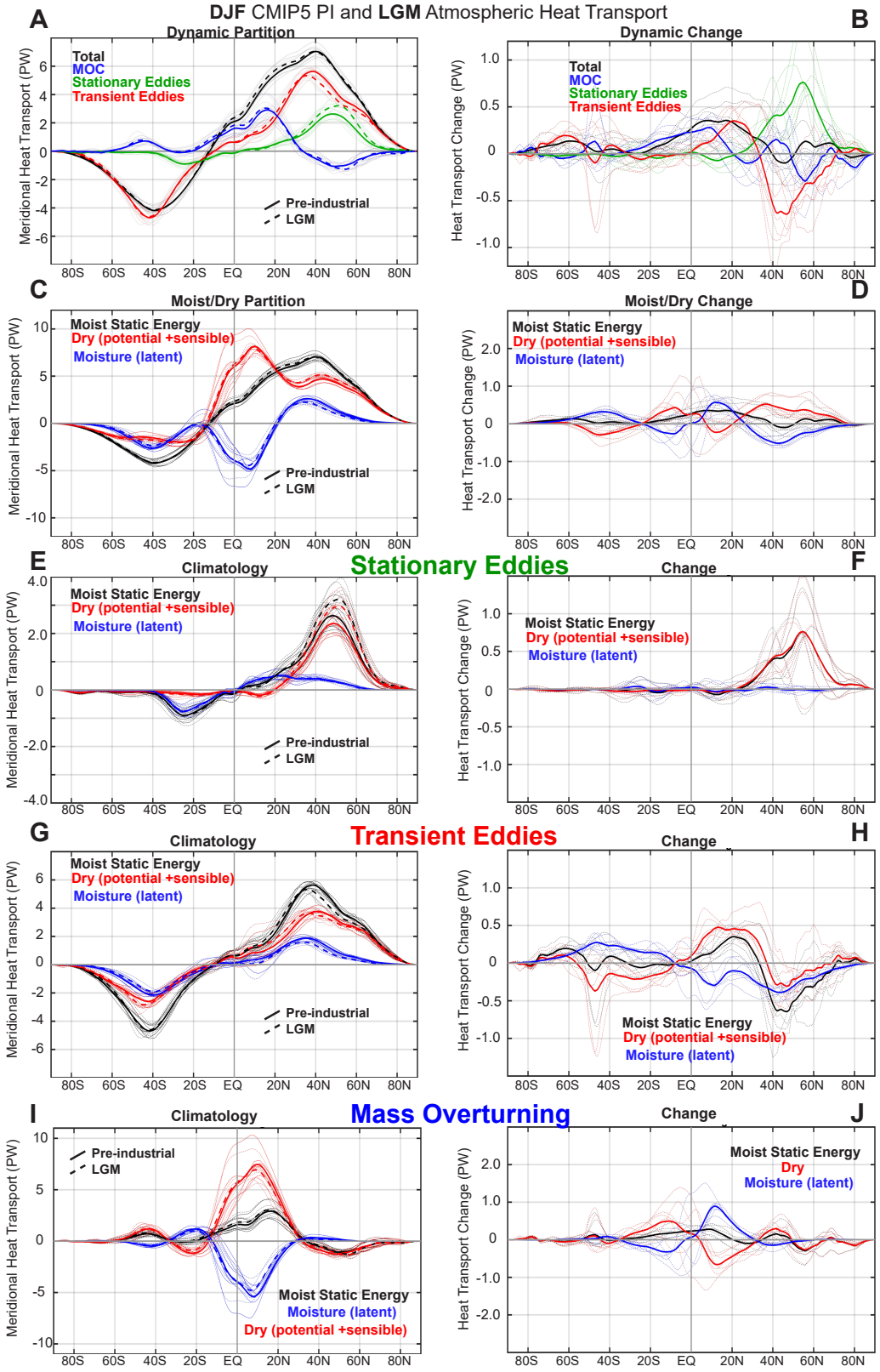


FIG. 9: As in Fig. 8 except for December/January/February. Note that the range on the y-axis has been doubled relative to Figure 8 in the moist/dry partitioning (panels C and D), the MOC transport (panels I and J) and the climatological stationary eddy transport (panel E)

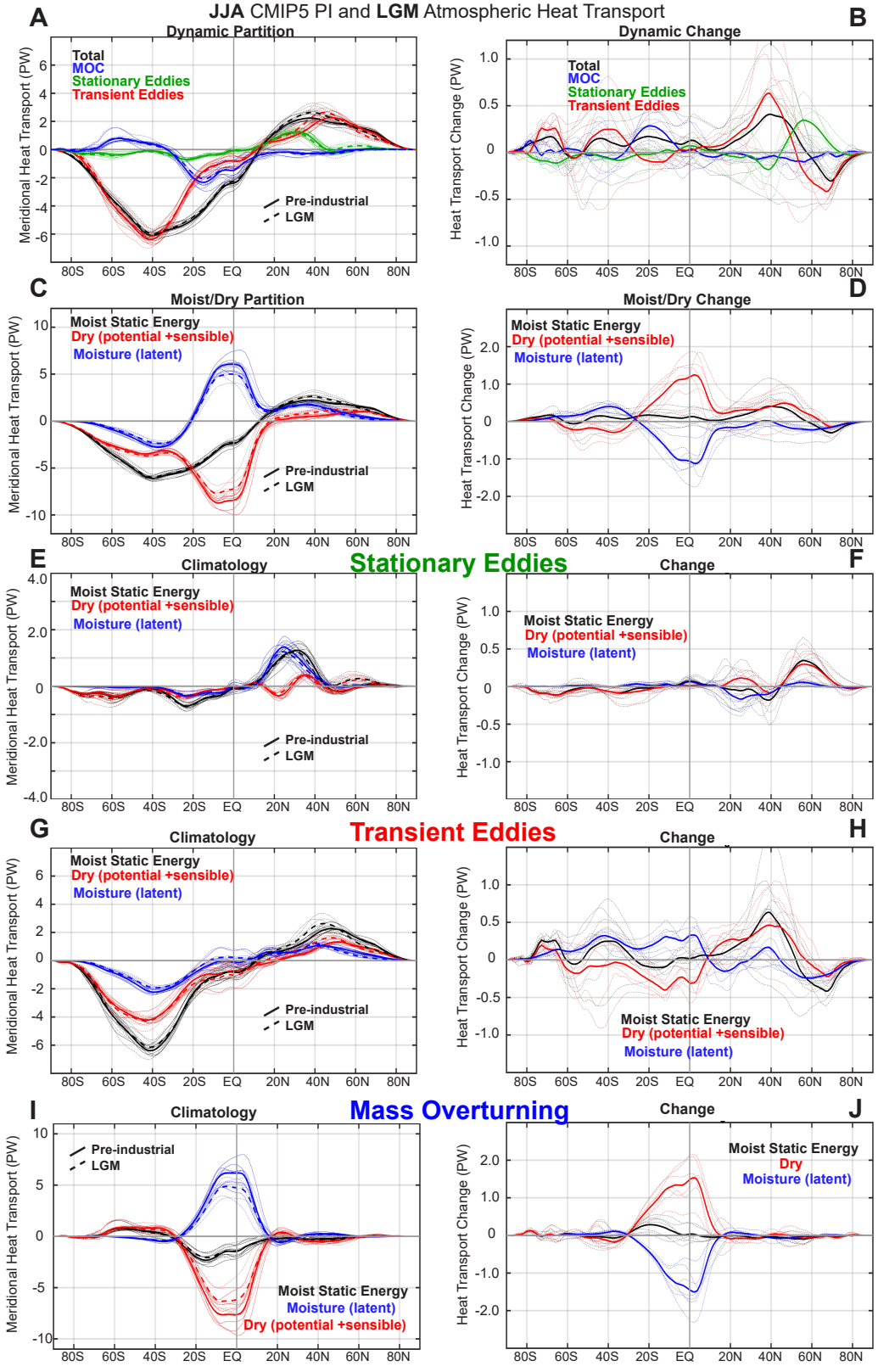


FIG. 10: As in Fig. 8 except for June/July/August.